Numerical modeling of light absorption and radiative forcing impacts of biomass burning emission proxies undergoing aqueous chemistry and photolysis

Alexandra E. Ng

4/1/2021

Department of Civil, Environmental and Geodetic Engineering

Advisor: Dr. Andrew May

Approved by:

Signature:

_____

Approved by:

Signature:

_____

Table of Contents

Abstract

Understanding and predicting climate change is essential to building knowledge for policymaking, engineering, and public health. Recent wildfires in the western United States resulted in biomass burning (BB) emissions that directly impacted regional air quality, and indirectly impacted climate change. However, quantifications of BB radiative forcing are uncertain. BB emits black carbon and various organic compounds ranging from particulate organic carbon to volatile organic compounds (VOC). Water soluble VOCs, including oxygenated aromatic compounds, can enter cloud water, in which they may undergo aqueous chemistry in cloudy atmospheres to form secondary organic aerosols (SOA). SOA contribute to radiative forcing by reflecting light (net cooling) or absorbing light (climate warming) when radiation is released as thermal energy.

The objective of this study was to model and predict absorption to quantify the climate warming effects of BB emission chemistry. Three MATLAB scripts were developed and tested for analysis of BB emission proxies using absorption values from another study. The first code fit experimental data to quantify the imaginary refractive indices (related to light absorption and warming) of the compounds and identified the absorbing and warming effects of the colored compounds produced. The second code modeled absorbance changes as chemical processes occurred over time. The third code modeled nonlinear imaginary refractive indices and absorbance changes over time. The codes successfully modeled the imaginary refractive indices with experimental data and predicted absorbance chemistry of some BB SOA. Absorbance experiments were deferred due to technical complications. A procedure to measure absorbance for modeling inputs was created for future experimental work. A solar simulator will be used to irradiate oxygenated aromatic compounds produced in BB (phenol, furfural, and benzaldehyde). The solar simulator imitates natural sunlight and requires calibration using a chemical actinometer such as ferrioxalate, a photosensitive iron oxide solution. A portable darkroom was constructed to prevent photodegradation of ferrioxalate. Calibration and experiments will be performed in the same method to minimize discrepancies. Six cuvettes will be filled with solution and irradiated in the solar simulator. The cuvettes will be removed at specific time points and the spectral absorbances will be measured using a UV-vis spectrometer. Finally, the absorbance and imaginary refractive index results will be implemented into the models to quantify radiative forcing impacts.

Acknowledgments

Firstly, I would like to thank Dr. May for advising this project and providing wonderful mentorship and guidance throughout my undergraduate research studies. I am grateful for his continuous support, from introducing me to air quality research to aiding in my graduate school pursuits.

In addition, I would like to thank July Laszakovits for her time, knowledge, and assistance with the solar simulator and ferrioxalate experiments. I want to thank Hrithik Basu for his assistance in and out of the laboratory.

Finally, I would like to thank Dr. Weavers for participating in my undergraduate research thesis defense committee.

List of Figures

Figure 17: *Kinetic model for catechol*

Figure 18: *Kinetic model for benzaldehyde*

List of Tables

List of Abbreviations

BB: biomass burning

BC: black carbon

BrC: “brown” carbon

DI: deionized

k: imaginary refractive index

n: real refractive index

PM: particulate matter

POA: primary organic aerosol

SOA: secondary organic aerosol

VOC: volatile organic compound

List of Equations

1. Introduction

In the past few years, extreme biomass burning (BB) events in the Western United States and Australia have destroyed homes, altered sensitive ecosystems, and released a variety of potentially harmful atmospheric pollutants on a regional scale. In some fires, BB emissions are capable of long-range transport, driven by microphysical properties of the emitted aerosols and atmospheric conditions (Dahlkötter et al., 2014). In all fires, regardless of the transport length, BB emissions are influenced by chemical evolutions of the smoke and aerosols, including chemical formation pathways, reaction kinetics, and secondary reactions (Hennigan et al., 2011). The complex chemical and physical transformations of BB emissions demonstrate the additional considerations that must be accounted for concerning the global environment and climate change. This is a growing concern, especially because quantifications of biomass burning climate impacts are uncertain. This project aims to address these issues by creating numerical models that can predict chemical kinetics and climate warming components of biomass burning emissions.

1.1. General Overview

Biomass burning can emit primary organic aerosols (POA) such as volatile organic compounds (VOC), particulate matter (PM), and black carbon (BC) (Lee et al., 2014). Within the atmosphere, water-soluble oxygenated aromatic VOC can be oxidized and undergo aqueous chemistry to form secondary organic aerosols (SOA) and “brown carbon” (BrC) (Laskin et al., 2015). Human health and climate changes are affected by primary and secondary aerosol emissions from BB (Hatch et al., 2015).

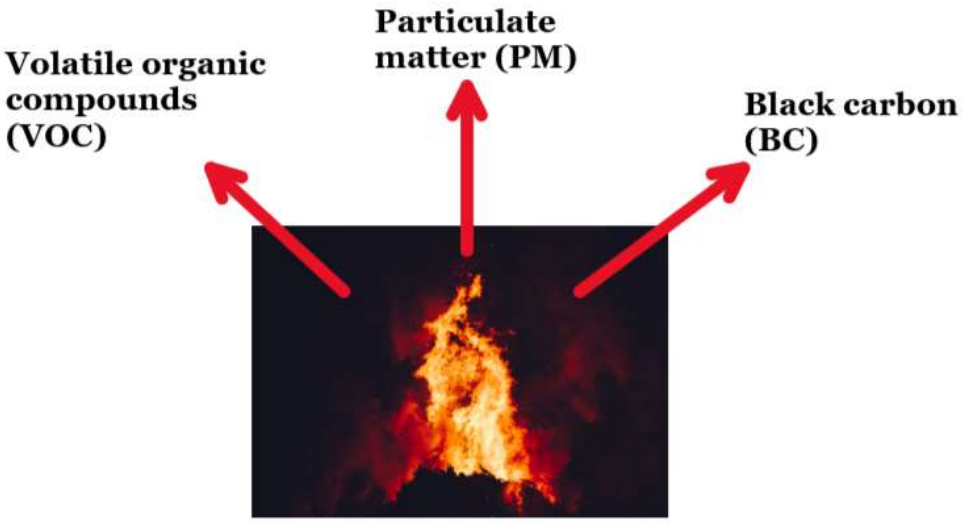

Figure 1: *Biomass burning emissions include a variety of atmospheric constituents including volatile organic compounds, particulate matter, and black carbon.*

Furthermore, atmospheric chemistry and climate change are influenced by direct and indirect interactions of atmospheric aerosols (Hatch et al., 2015). Atmospheric aerosols can contribute to climate warming through aerosol absorption when radiation is released as thermal energy (Laskin et al., 2015). Aerosol scattering results in climate cooling when radiation is reflected back into space (Seinfeld & Pandis, 2016).

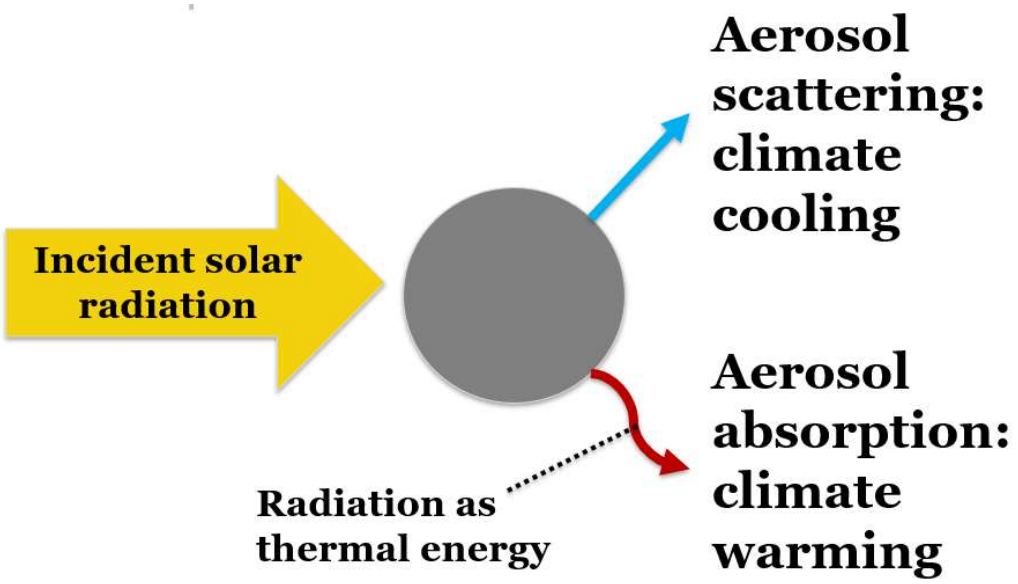

Figure 2: *Climate impacts from solar radiation interaction with particles.*

Due to the potential radiative forcing from SOAs, it is important to understand the optical properties and aqueous chemistry (Lee et al., 2014). By measuring colored products produced by irradiating BB emissions, the photochemical kinetics and photolysis of aerosols undergoing aqueous chemistry can be quantified (Smith et al., 2016).

In a 2010 study by Chang and Thompson investigated the kinetics of phenolic compounds and the formation of colored products. Their research tested a variety of organic compounds including and determined that phenols are commonly found at higher concentrations in emissions and may be significant in the formation of colored products (Chang & Thompson, 2010).

1.2. Secondary organic aerosols

SOA can be formed through oxidation processes of VOCs in the atmosphere. These VOCs can be attributed to both anthropogenic and natural biogenic sources (Laskin et al., 2015). Vegetation can contribute to direct emissions of biogenic VOCs. Biomass burning combustion of vegetation contributes to global VOCs. Anthropogenic VOCs are sourced from vehicular emissions, biomass burning, or oil drilling with all VOCs can be considered as SOA precursors (Shrivastava et al., 2017). There are different classifications of SOA volatility types ranging from extremely low volatility organic compounds to semi-volatile organic compounds (Shrivastava et al., 2017).

Many studies have determined that SOA often dominates atmospheric organic aerosol, since POA tends to only be relevant near source regions such as urban areas. This highlights the importance of understanding SOA formation (Jimenez et al., 2009; Tuet et al., 2017). VOCs with more carbon atoms and oxidized molecules have relatively low vapor pressures and have a greater tendency to produce SOAs than those with higher vapor pressures. Therefore, the quantification of SOA production from oxidized VOCs is essential to creating accurate emission inventories. Furthermore, global SOAs are generally underestimated in atmospheric models (Zhang et al., 2007).

1.3. Aqueous chemistry and photolysis

The presence of clouds and/or fog in the atmosphere can result in aqueous chemistry after a VOC partitions from the gas to aqueous phase (Smith et al., 2016). Water soluble compounds such as phenols and aromatics are more likely to partition into atmospheric water, where they can be oxidized and form SOA (Lee et al., 2014).

The water in clouds can influence the reactivity and kinetics of compounds during SOA formation, impacting water uptake by particles (Shrivastava et al., 2017). As a result, aqueous atmospheric particles are important for considerations into the potential impacts on cloud nucleation and cloud microphysics (Duarte et al., 2007).

The chemical process of SOA production in the aqueous phase involves oxidation by hydroxyl radicals (OH) and photolysis can occur to form radicals (Smith et al., 2016). To produce reactive OH for radical chemistry in a laboratory setting, hydrogen peroxide (H2O2) can be irradiated to produce two hydroxyls (Chang & Thompson, 2010).

1.4. Light-absorbing carbon

BC is a well-known light-absorbing organic aerosol that is sourced from BB and combustion (Laskin et al., 2015). The complex properties of BC, such as chemical structure and optical properties, have been characterized and are somewhat constrained.

BrC is another light-absorbing organic aerosol. However, the understanding of light absorption by BrC particle is significantly more dependent on wavelength than BC (Shrivastava et al., 2017). BrC can be not only emitted directly from biomass burning and other forms of combustion (Lee et al., 2014) but also produced through atmospheric chemistry, such as the oxidation of phenolic and aromatic compounds. While BC is also produced by biomass burning, BrC absorbs more blue light while BC absorbs more red light (Chylek et al., 2019). BrC is an aerosol that absorbs light linearly with increasing wavelengths (Shrivastava et al., 2017). Due to the wavelength dependence of BrC, the optical properties of BrC are important for radiative forcing characterization (Shrivastava et al., 2017). Even so, BrC consists of different compounds

in the form of a complex mixture, demonstrating the intricacies of identifying the composition of BrC (Chang & Thompson, 2010). Therefore, quantifying the global radiative forcing contribution from BrC is necessary for inclusion in climate models and emission contents.

1.5 Aerosol interactions with light

The small particle interactions with light can be characterized by the scattering of electric charge in all directions or the conversion of radiation to thermal energy through absorption (Seinfeld & Pandis, 2016). Mie theory is a formulation that describes the process of small homogenous spherical particle light scattering. Mie theory also allows for simplified calculations of optical particle properties (Fan et al., 2014). As a result, the refractive index (N) can be defined as (Seinfeld & Pandis, 2016):

$$N = n + ik$$

Equation 1: *The refractive index (N) is composed of the real refractive index (n), the imaginary refractive index (k), and the unit imaginary number (i).*

The real refractive index is the reflective or nonabsorbing component of the refractive index. The imaginary refractive indices of a compound quantifies the absorption of an aerosol (Laskin et al., 2015).

The following equation can be used to quantify the imaginary refractive indices (Sun et al., 2007):

$$k = \frac{\ln(10)}{4\pi}\frac{\rho\lambda}{cL}A(\lambda)$$

Equation 2: *Imaginary refractive index (k) can be calculated with the equation above.*

The inputs includes material density (ρ), wavelength (λ), concentration (c), optical path length (L), and absorbance (A) (Liu et al., 2015). This equation allows the imaginary refractive index to be derived from UV-visible spectroscopy absorbance measurements.

1.6. Climate impacts and radiative forcing

Aerosol scattering and absorption are important properties that can be quantified with the refractive index to analyze climate impacts and radiative forcing from SOA. Particles with only a real term in their refractive index will have a net cooling effect, excluding cloud properties and surface reflection, while particles with a non-zero imaginary refractive index may have a net warming effect (Laskin et al., 2015). Within clouds, reflectivity of solar radiation by droplets will result in climate cooling while absorbing aerosols are contribute to climate warming (Duarte et al., 2007; Laskin et al., 2015). Atmospheric aerosol affect radiative forcing, however, extensive uncertainty remains due to physical and chemical evolutions of aerosols (Jimenez et al., 2009).

1.7. Objectives

Biomass burning emits many oxidized aromatic compounds that can partition into cloud water and undergo aqueous chemistry to produce BrC. Therefore, the evident need for understanding BB impacts to climate change is clear. As a result, the motivation for this study was to address these uncertainties. This study was conducted to:

- Model imaginary refractive indices (absorption and warming component) fitting of BB compounds
- Predict BB compound absorbance changes and chemistry over time
- Create an experimental methodology for future work
- Determine radiative forcing impacts

2. Methods

MATLAB code was developed to create a model that quantifies the imaginary refractive indices of compounds based on absorbance values. The imaginary refractive index is the absorbance component of radiative forcing. In a 2010 study, Chang & Thompson measured absorbance of 12 phenolic BB compounds through experimental irradiation. These experimental absorbance values were in the development of MATLAB code to fit, model, and predict reaction kinetics and imaginary refractive indices. The following sections provide descriptions of three models created in MATLAB, including the inputs, outputs, and equations utilized. The actual MATLAB code for these models can be found in *Appendix 2*.

2.1. Linear fitting of imaginary refractive indices with absorbance values

The first step was to write code in order to determine which BB compounds followed linear increases with imaginary refractive indices. This code creates a linear graph of best fit for the imaginary refractive indices for 12 BB emission compounds (phenol, p-hydroxybenzaldehyde, guaiacol, vanillin, syringol, 4-methylsyringol, syringaldehyde, pyrogallol, catechol, resorcinol, 3,4-dimethoxybenzaldehyde, and benzaldehyde). The code inputs include molecular weight of the compounds as well as absorbance and time values for the 12 compounds, from the Chang and Thompson experiment. This code uses the assumptions that optical path length is 0.01 m, material density is 1400 kg m^{-3}, and wavelength is 450 nm. The optical path length is based on a standard cuvette length of 1 cm that is commonly used in a UV-Vis. The material density was based on previous studies (Liu et al., 2015). A wavelength of 450 nm assumes a blue-tone light, which BrC may readily absorb. The following equation was used to calculate the imaginary refractive index (k) of the experimental absorbance data:

$$k = \frac{\ln(10)}{4\pi}\frac{\rho\lambda}{cL}A(\lambda)$$

Equation 2: *The imaginary refractive index (k) is calculated with material density (ρ), wavelength (λ), concentration (c), optical path length (L), and absorbance (A) (Liu et al., 2015).*

This code utilized MATLAB functions *polyfit* and *polyval* to determine the line of best fit. The *polyfit* function was used to determine a linear fit for the calculated imaginary refractive indices. The inputs for the *polyval* function included time,

coefficients from the *polyfit* function, and the polynomial degree. The *polyfit* function also outputs a structure, S, that can be inputted into *polyval* to determine error estimations. The *polyval* function uses the coefficient and error structure outputs of the *polyfit* function to evaluate the polynomial for each point in the time vector. This outputs the best fit imaginary refractive indices and the standard error. The standard error was calculated by summing the error for each value. The outputs of the code include imaginary refractive index (k) and graphs for all 12 compound with k vs. time (*Figure 1a in Appendix 1*). The code can be found in *Appendix 2a*.

2.2. Nonlinear modeling of absorbance

The purpose of this code was to determine time constants that generate a nonlinear graph of best fit for absorbance. This code creates nonlinear graphs of best fit for absorbance for 12 BB emission compounds. The code inputs include molecular weight of the compounds. Additional inputs for the 12 compounds include absorbance, time vector, initial time, and maximum absorbance values, from the Chang and Thompson experiment. The following equation was used to model absorbance based on the apparent functional form of those data:

$$\frac{dA}{dt} = A_{max} * (1 - e^{-\frac{t}{\tau}})$$

Equation 3*: Absorbance (A) is calculated with maximum absorbance (A_{max}), time (t), and time constant (τ).*

This code utilized MATLAB functions *lsqcurvefit* and *polyval* to determine the value of the time constant that produces the line of best fit. The *lsqcurvefit* function was

used to find the coefficients to fit the nonlinear function (Equation 3) to the experimental absorbance data. The *lsqcurvefit* function returns fitting coefficients and squared sum of the differences of the fit. The standard deviation was calculated bt taking the square root of the residual sum divided by the data size. Standard error was calculated by dividing the standard deviation by the square rot of the mean absorance values. The outputs of the code includes graphs for all 12 compound with Absorbance vs. time (*Figure 1b in Appendix 1*). The code can be found in *Appendix 2b*.

2.3. Determining global minimum error for time constant

In the nonlinear model, the time constant was determined to create the best fit absorbance values. The *lsqcurvefit* function determines the local minimum error instead of the global minimum error for the fitting equation. Therefore, graphs for initial time constant values ranging from 1 to 1000 or 1 to 10,000 minutes were created to determine the initial time constant for the global minimum error. The same equation from the nonlinear fit (*Equation* 3) was used and input into the *lsqcurvefit* function.

The outputs included the value for the time constant of best fit and the residual error sum. For each of the 12 compounds, two graphs are created. The first graph plots the initial time constant input for the fit on the x axis and the residual sum error on the y axis. The second graph plots the predicted time constant for the fit on the x axis and the residual sum error on the y axis. The values of the time constant for the graphs were used in the kinetic models.

2.4. Kinetic models

The kinetic model was created to determine which compounds followed a nonlinear model for absorbance and imaginary refractive index. This code creates graphs for compound degradation, imaginary refractive index, and absorbance over time for phenol, guaiacol, vanillin, syringol, catechol, and benzaldehyde. The other compounds did not have experimentally derived rate constants so they were not included in this model. The coupled model inputs include molecular weight, rate constant, maximum absorbance, and initial time constant values (from *Section 2.3*) for the compounds. The model assumes an initial test compound concentration of 10^{-6} M and initial H_2O_2 concentration of 1^{-6} M.

$$\frac{dA}{dt} = A_{max} * (1 - e^{-\frac{t}{\tau}})$$

Equation 3*: Absorbance (A) is calculated with maximum absorbance (A_{max}), time (t), and the calculated time constant (τ).*

The H_2O_2, OH, test compound concentration, and time constant values are estimated using Eulers's method to numerically approximate absorbance using the initial concentration and a time step. This model outputs three graphs for each compound including concentration over time, absorbance over time, and imaginary refractive index over time.

2.5. Climate impact calculations

A code was developed that calculates the extinction, scattering, and absorption efficiency for an aerosol size distribution as well as the single-scattering albedo (SSA). SSA can be used to calculate radiative forcing and climate impacts. The efficiency values are calculated by running an aerosol optics code that was developed by Cappa et al. (Cappa et al., 2012). The aerosol size distribution was calculated by creating an array of diameters ranging from the ultrafine to fine range (100 to 1000 nm particle diameter). The parameters for the aerosol size distribution included a geometric mean diameter of 200 nm, geometric standard deviation of 1.5 and a paricle number concentration of 3000 per cm^3. The size distribution was calculated with log10 spacing using the following equation:

$$\frac{dNdlog10}{dp} = \frac{N}{\sqrt{2 * \pi * log_{10}(\sigma_g)}} * \exp\left(\frac{-\left(log_{10}(dp) - log_{10}(dpg)\right)^2}{\left(2 * log_{10}(\sigma_g)\right)^2}\right)$$

Equation 4*: The equation above calculates the aerosol size distribution with log10 spacing with the particle number concentration (N), geometric standard deviation (σ_g), and geometric mean diamter (dpg).*

The inputs for the aerosol optics code includes wavelength of light, real refractive index of aerosol, imaginary refractive index of aerosol (from fitting code), and particle diameter distribution. The code assumes Mie scattering, 450 nm wavelength, and a real refractive index of 1.55 (Bohren & Huffman, 1998).The outputs include extinction, scattering, and absorption efficiencies for each particle diameter. The extinction,

scattering, and absorption efficiency coefficients for each particle diameters are calculated with the following equation using the outputs from the aerosol optics code:

$$b_{ext} = (\pi * dp * 10^{-9})^{2/4} * q_{ext} * dNddp * 10^{6}$$

$$b_{sca} = (\pi * dp * 10^{-9})^{2/4} * q_{sca} * dNddp * 10^{6}$$

$$b_{abs} = (\pi * dp * 10^{-9})^{2/4} * q_{abs} * dNddp * 10^{6}$$

Equation 5*: The equation above calculates the extinction, scattering, and absorption coefficients (b) at each particle diameter (dNddp) using particle diameter (dp) and the extinction, scattering, absorption efficiency outputs from the aerosol optics code.*

The SSA was calculated with the following equation:

$$SSA = \frac{B_{sca}}{B_{ext}}$$

Equation 6*: The equation above calculates the single-scattering albedo (SSA) with the scattering coefficient (B_{sca}) and extinction coefficient (B_{ext}).*

2.6. Model verification

The three models created can be verified with experimental measurements of the same compounds under irradiation in laboratory experiments. Due to technical issues and timing limitations due to COVID-19, the experimental verification was deferred. Further discussion about experimental procedures can be found in the *Future Work* section of this paper.

3. Results

3.1. Linear fitting of imaginary refractive indices with absorbance values

For compounds such as phenol and catechol, the linear model closely predicted the imaginary refractive index. In certain instances, the assumption that the imaginary refractive index increased linearly was correct. Other compounds did not follow the linear assumption for imaginary refractive index.

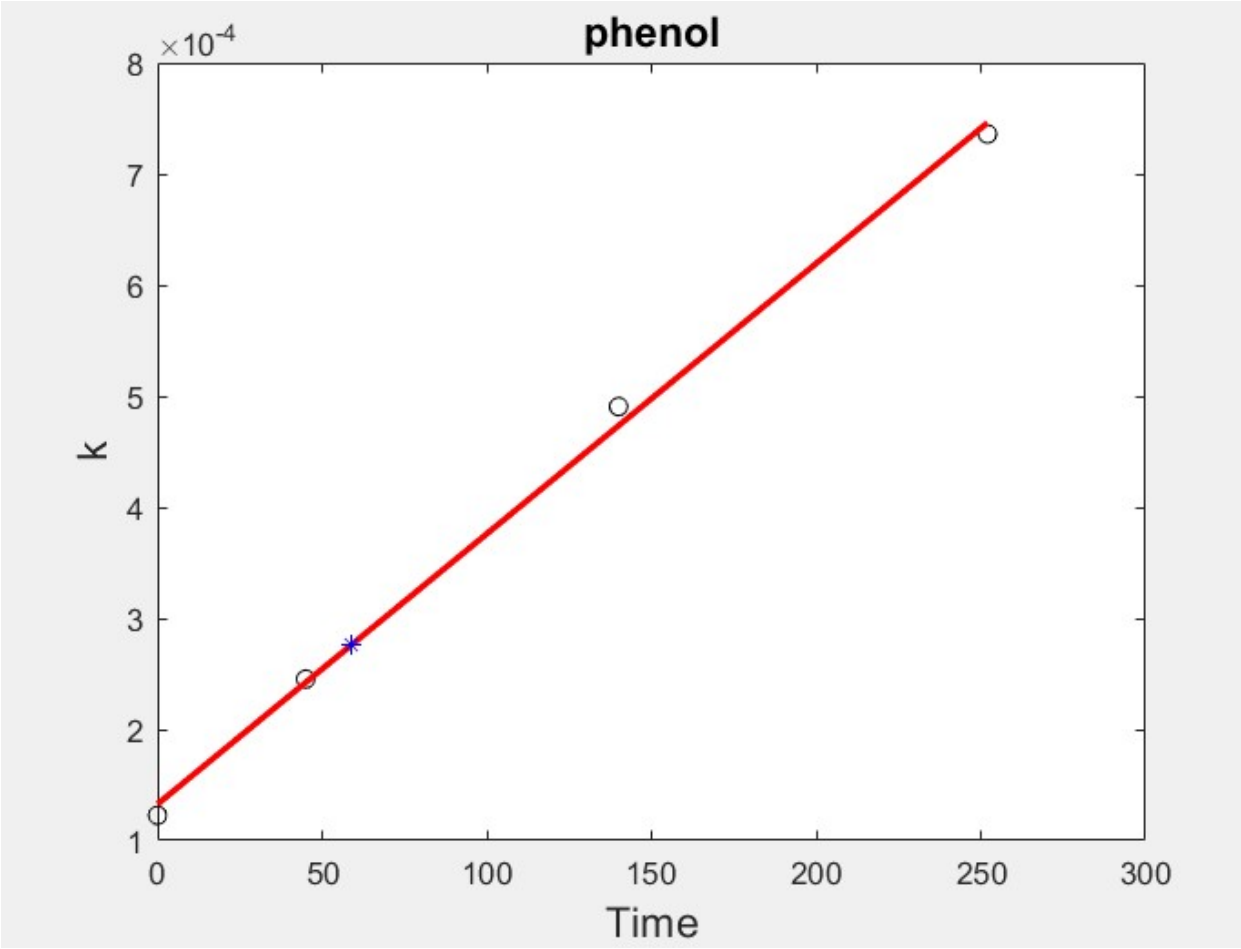

Figure 3: *Imaginary refractive index linear model for phenol*

The modeled imaginary refractive index for phenol followed the linear trend shown in the measured values from Chang & Thompson. The blue asterisk represents the predicted imaginary refractive index at one hour . The value for imaginary refractive index at one hour is important because it indicates the short term kinetics of the compounds. One hour can also approximate the lifetime of a single cloud droplet. At one hour, the imaginary refractive index of phenol is at approximately 2.76×10^{-4}. The linear fit for the imaginary refractive index for phenol over time followed the linear assumption.

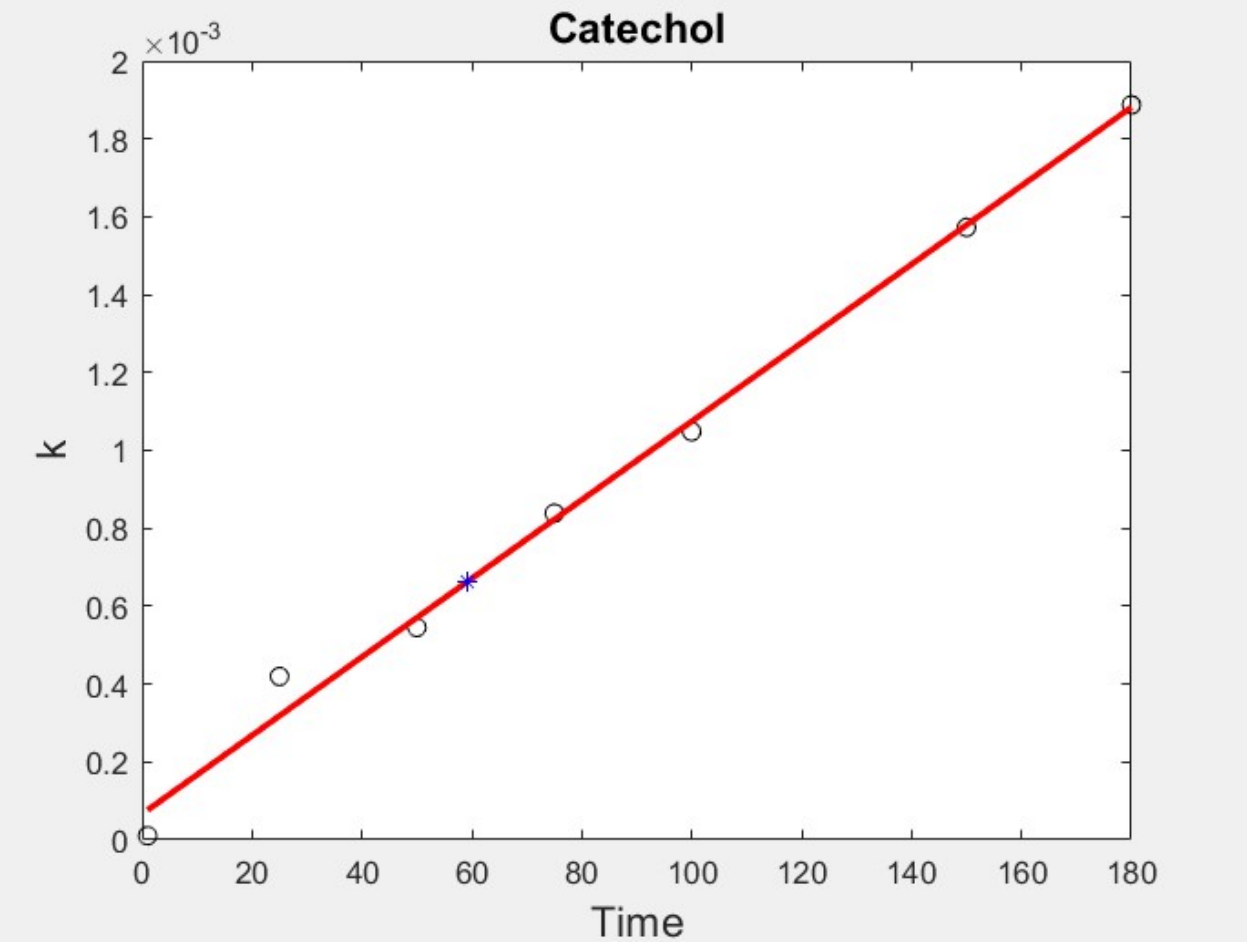

Figure 4: *Imaginary refractive index linear model for catechol*

Similarly, most measured values for imaginary refractive index aligned with the linear model for catechol. Catechol also followed the linear trend for imaginary refractive index. Catechol did not appear to reach a steady-state concentration. At one hour, the model predicts the imaginary refractive index of catechol to be 6.62×10^{-4}.

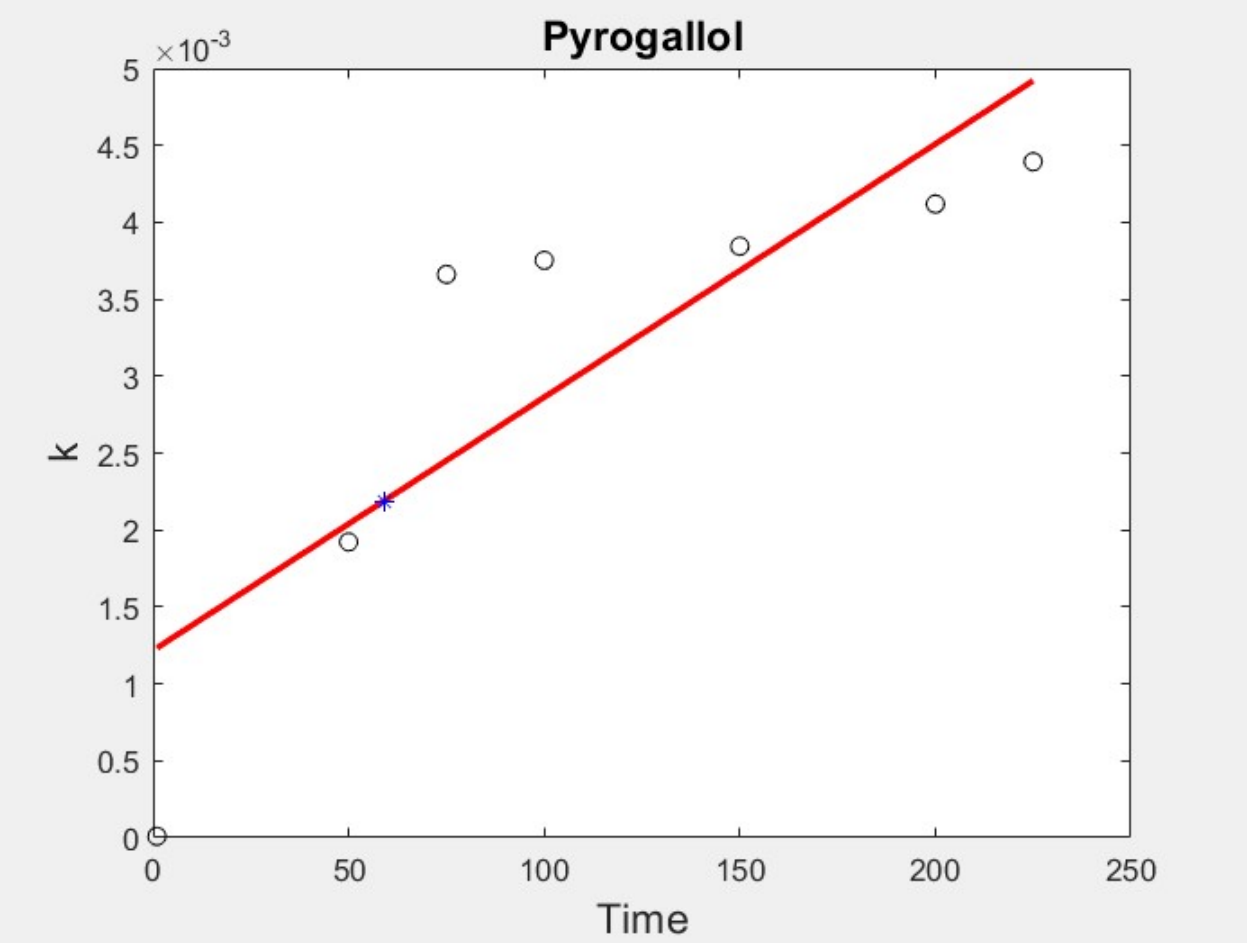

Figure 5: *Imaginary refractive index linear model for pyrogallol*

Pyrogallol did not closely follow the linear assumption for imaginary refractive index. Instead, the imaginary refractive index reaches a relative steady state at around 75 minutes. The actual imaginary refractive index differs substantially from the

predicted linear results. The blue asterisk represents the predicted imaginary refractive index to be 2.196×10^{-3} at one hour for pyrogallol.

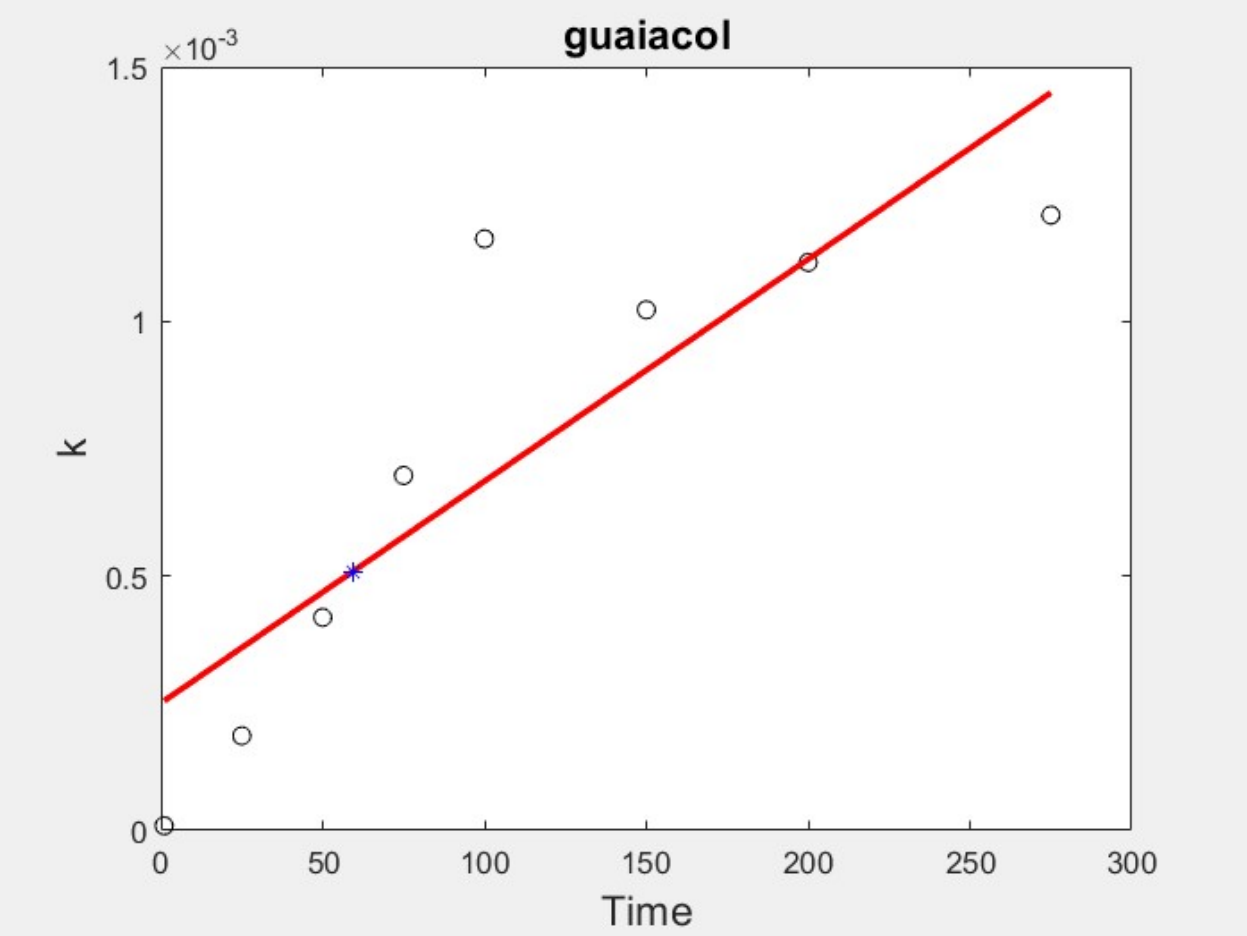

Figure 6: *Imaginary refractive index linear model for guaiacol*

The modeled imaginary refractive index for guaiacol also did not follow the linear trend shown in the measured values from Chang & Thompson. The blue asterisk represents the predicted imaginary refractive index at 5.08×10^{-4} at one hour for guaiacol. The actual imaginary refractive index differs substantially from the predicted linear results. Guaiacol also did not follow a linear trend for imaginary refractive index.

The imaginary refractive index reaches a relative steady state level at around 100 minutes.

3.2. Nonlinear modeling of absorbance

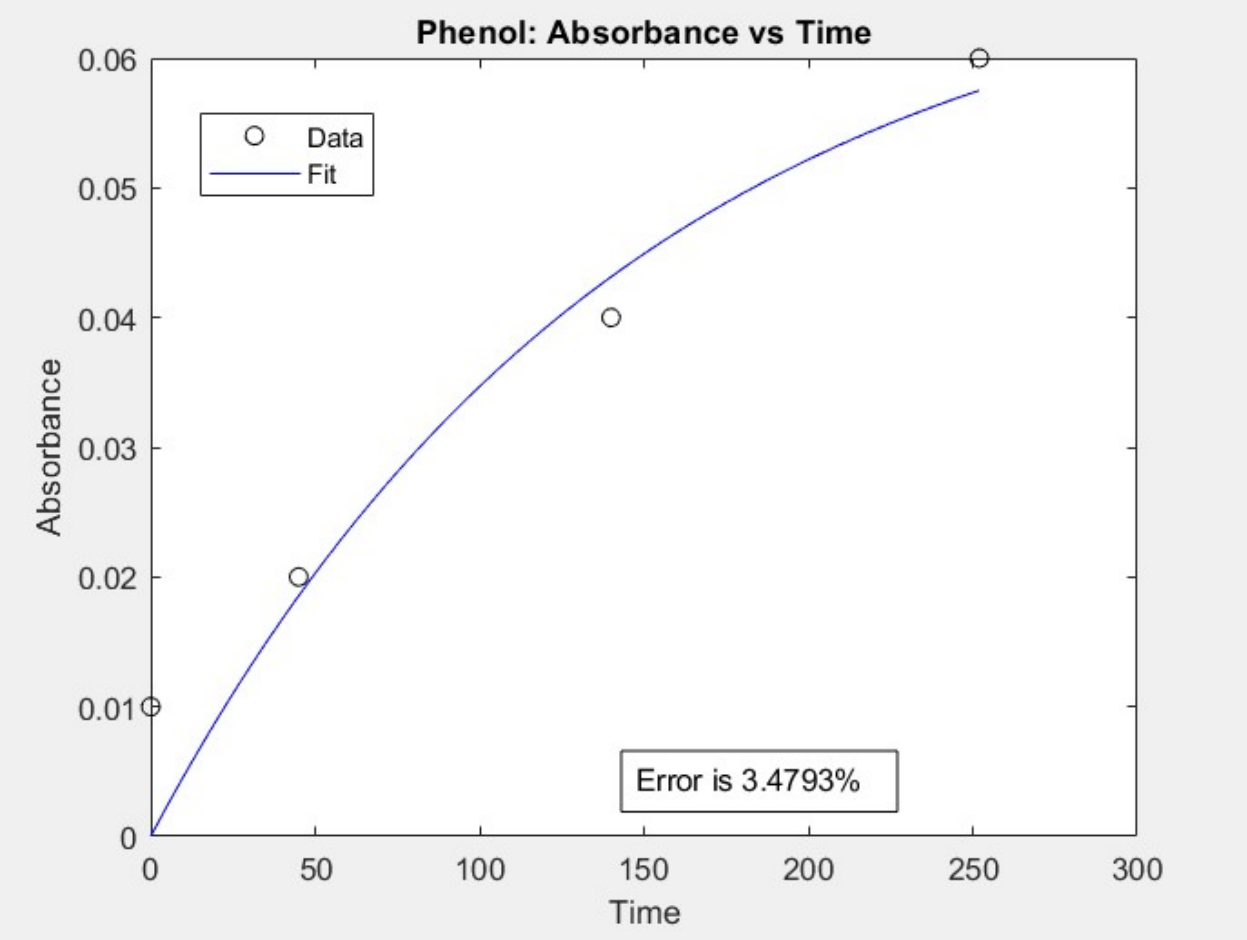

Figure 7: *Absorbance nonlinear model for phenol*

The absorbance fit for phenol followed the nonlinear fit for absorbance with a time constant of 146. Phenol does not reach a clear steady state. The nonlinear model assumes zero initial absorbance when the actual initial absorbance is non-zero.

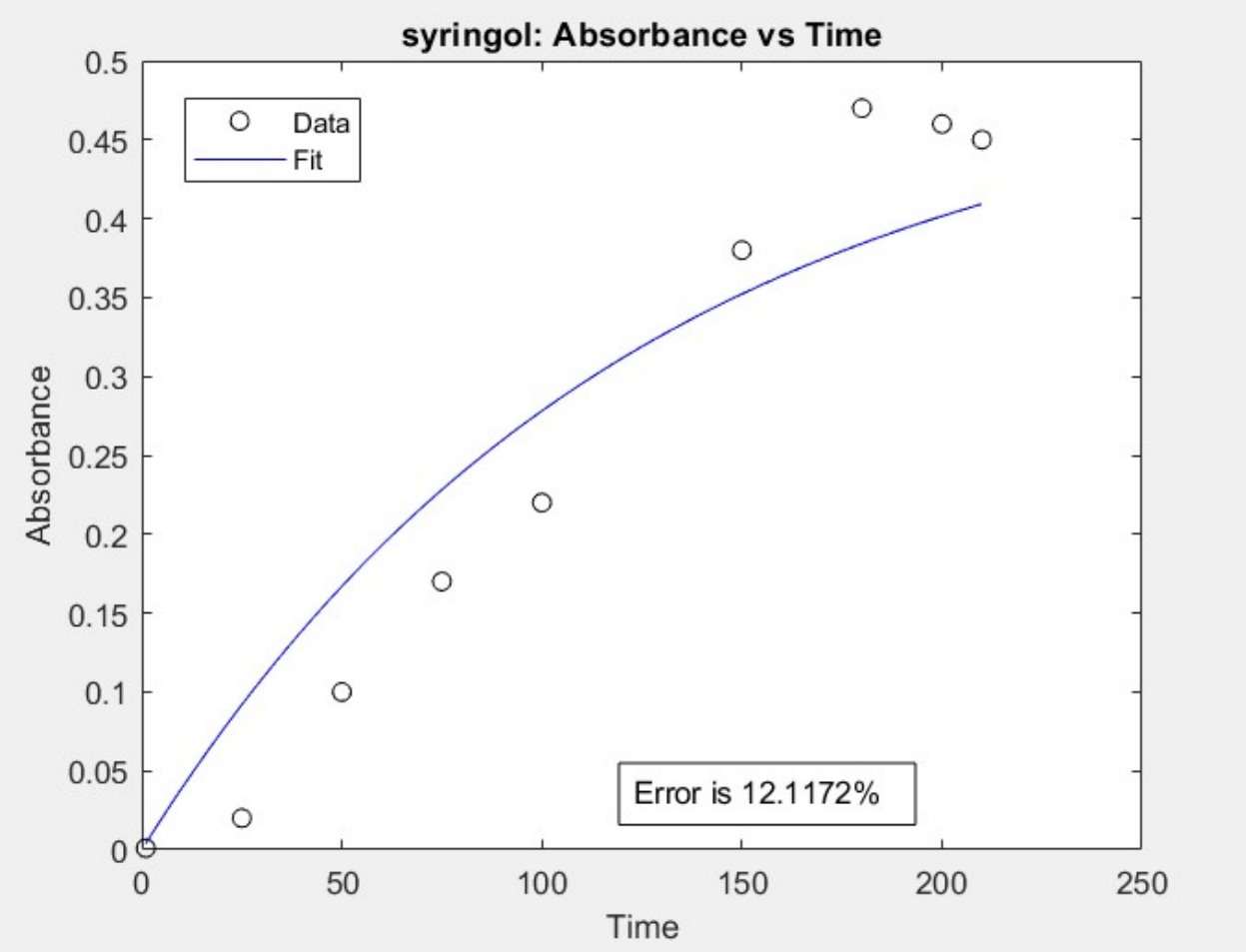

Figure 8: *Absorbance nonlinear model for syringol*

The absorbance fit for syringol did not follow the nonlinear fit for absorbance with a time constant of 123. The nonlinear model overpredicts absorbance until approximately 150 minutes. At 150 minutes, the model underpredicts absorbance for syringol. While syringol absorbance begins to decline at around 175 minutes, a clear steady state absorbance is not clearly evident.

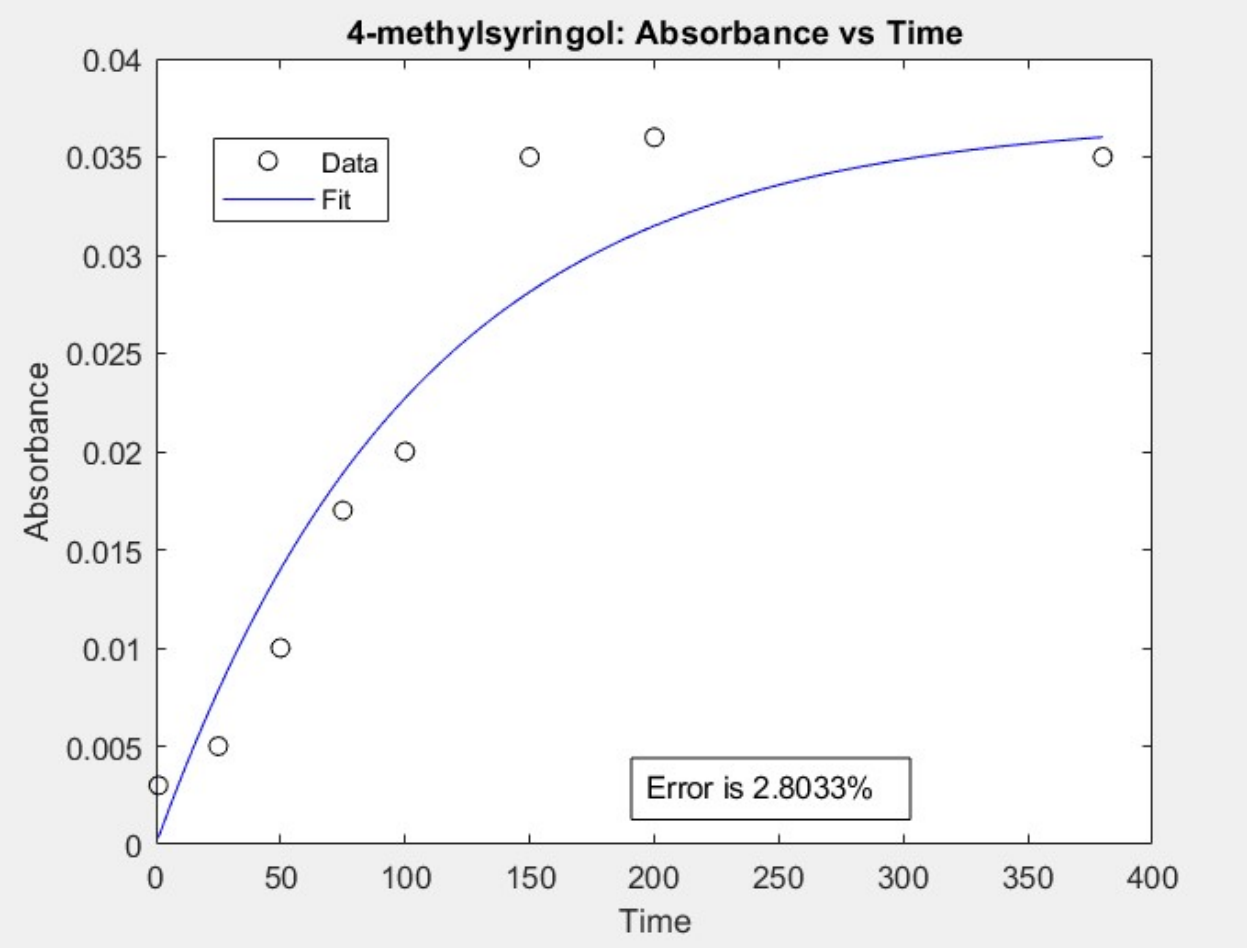

Figure 9: *Absorbance nonlinear model for 4-methylsyringol*

The nonlinear model for 4-methylsyringol followed the nonlinear trend until approximately 150 minutes. At 150 minutes, the model under predicts absorbance for 4-methylesyringol. Before 150 minutes, the model overpredicts absorbance. The absorbance fit for 4-methylsyringol did not exactly follow the nonlinear fit for absorbance with a time constant of 105 due to the assumed functional form for absorbance.

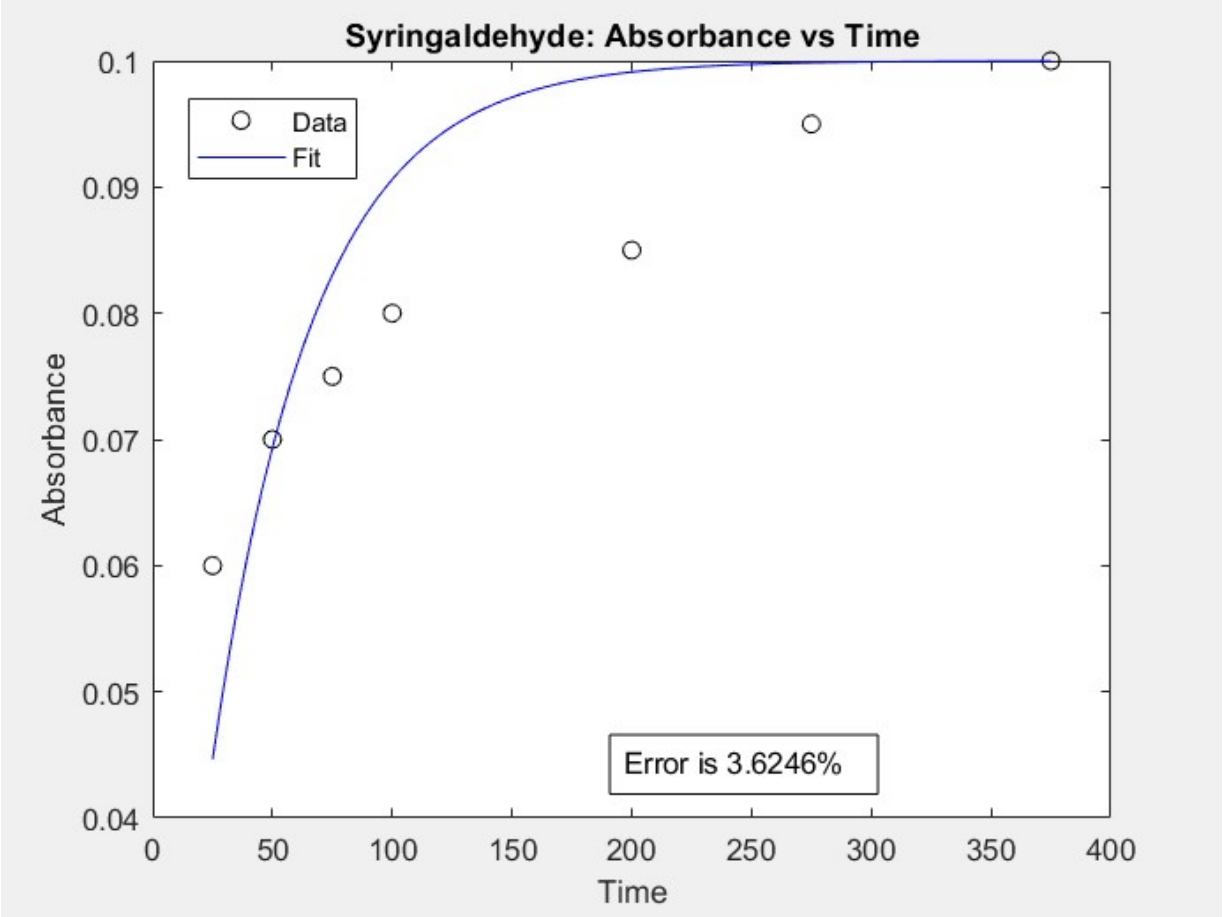

Figure 10: *Absorbance nonlinear model for syringaldehyde*

The absorbance fit for syringaldehyde did not follow the nonlinear fit for absorbance with a time constant of 42.1. At around 50 minutes, the model significantly overpredicts absorbance due to an assumption that initial absorbance is zero. Syringaldehyde does not reach a clear steady state but the model predicts steady state and maximum absorbance at approximately 200 minutes.

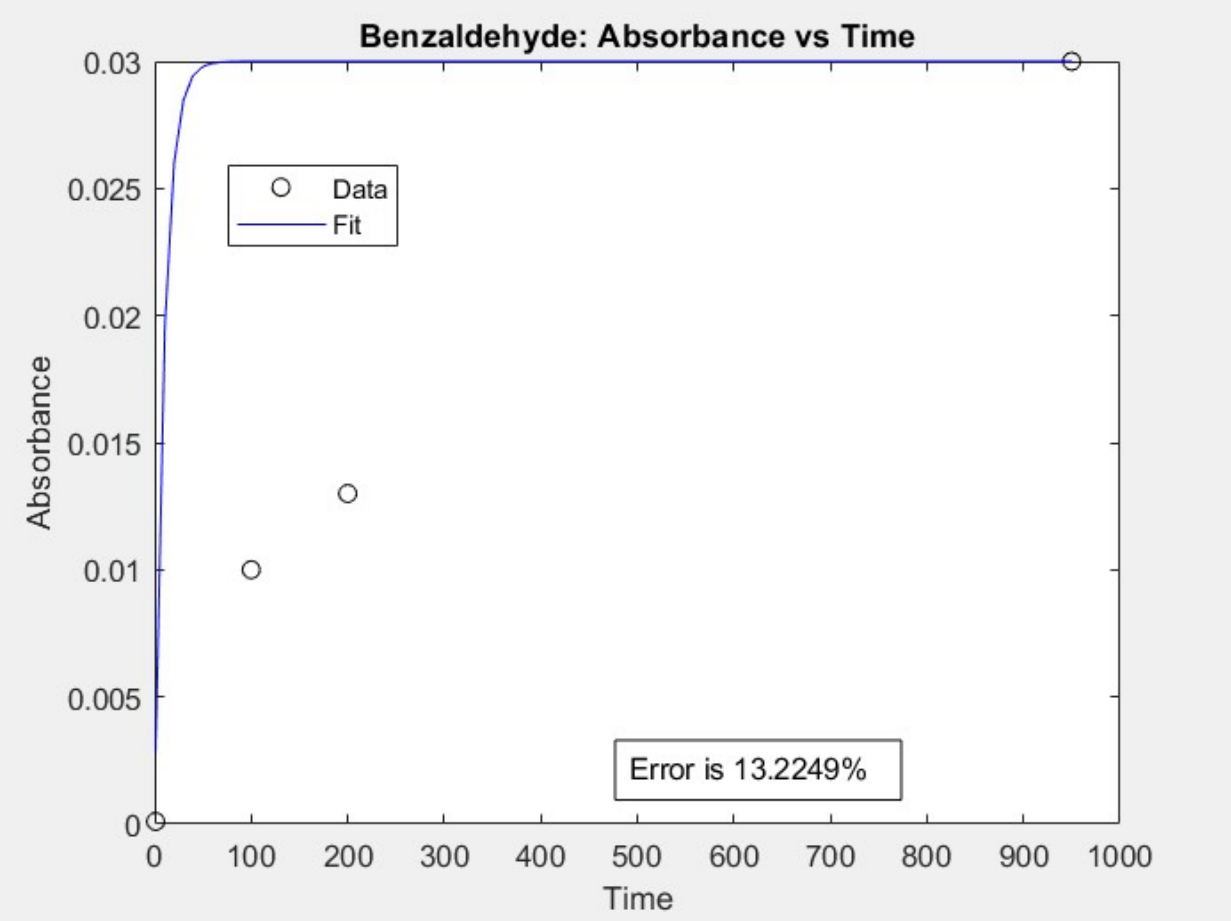

Figure 11: *Absorbance nonlinear model for benzaldehyde with set initial time constant*

The initial value of the time constant was arbitrarily set. Although this found nonlinear best fit models for most compounds but the set initial absorbance value did not result in a best fit nonlinear solution for benzaldehyde. The model significantly overpredicts absorbance for benzaldehyde and predicts that maximum absorbance is reached at around 75 minutes.

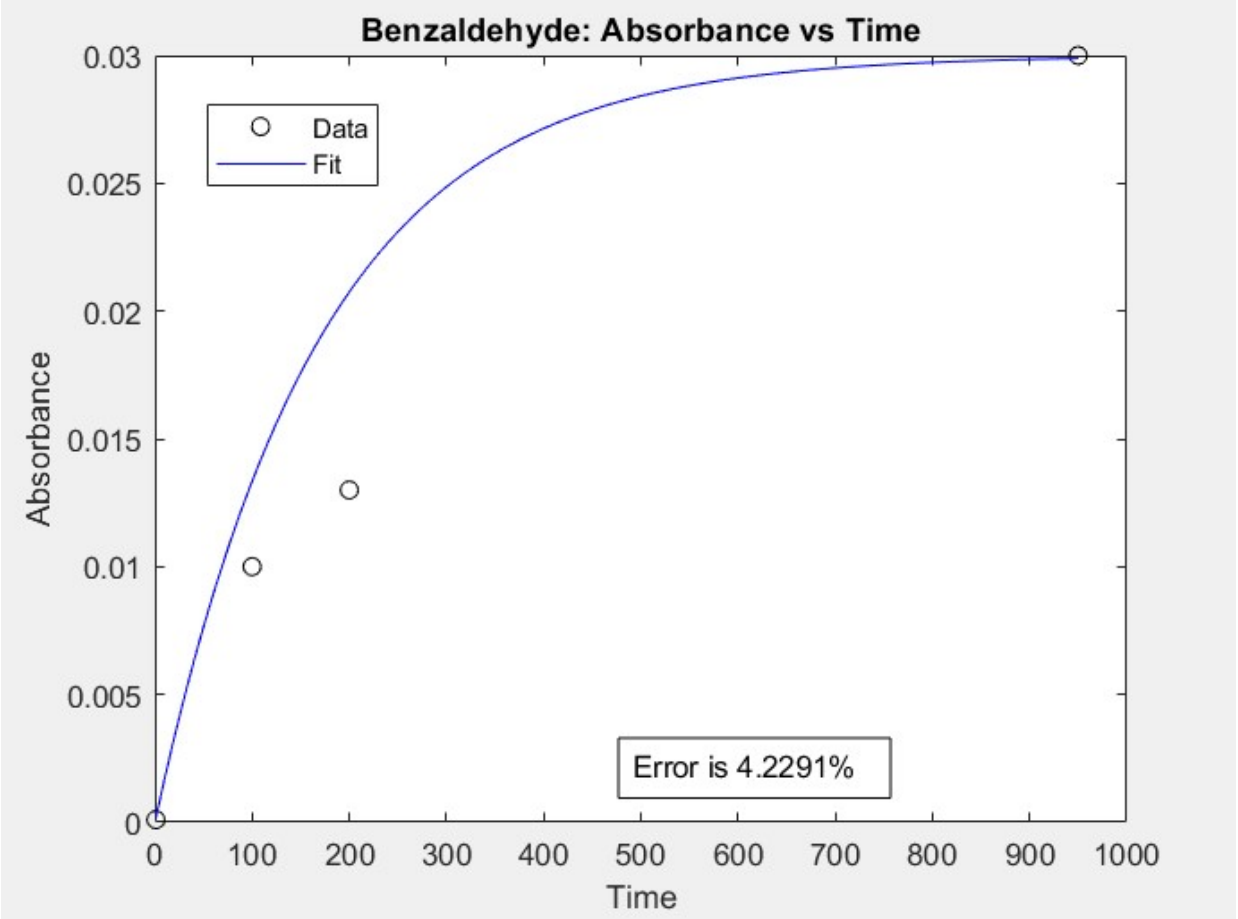

Figure 12: *Absorbance nonlinear model for benzaldehyde with adjusted initial time constant*

When the initial time constant value for benzaldehyde was increased, the nonlinear fit significantly improved with a greater time constant. Although the nonlinear model still overpredicts absorbance for benzaldehyde, the fit is improved.

The nonlinear model also predicted the time constant that was used to create the nonlinear line of best fit with *Equation 5*. The predicted time constants for the twelve compounds can be found in *Table 1* and *Table 2* below.

Table 1: *Predicted time constant for first 6 compounds*

Compound	phenol	p-hydroxybenzaldehyde	guaiacol	vanillin	syringol	4-methylsyringol
Time constant	146	59.5	82.9	118	123	105

Table 2: *Predicted time constant for second 6 compounds*

Compound	syringaldehyde	pyrogallol	catechol	resorcinol	3,4-dimethoxy-benzaldehyde	benzaldehyde
Time constant	42.1	66.6	113	113	156	170

3.3. Coupled model

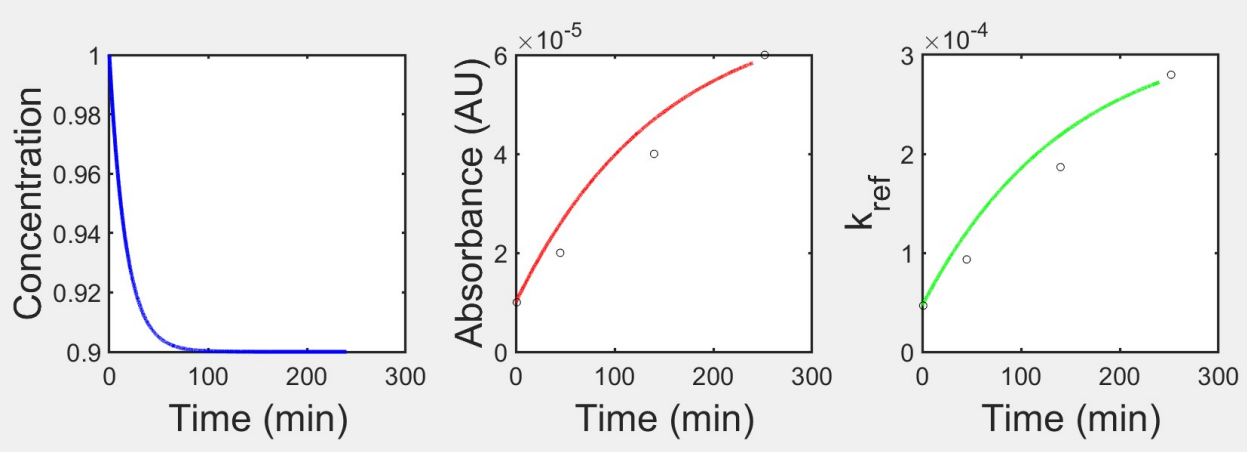

Figure 13: *Kinetic model for phenol*

Absorbance and imaginary refractive index appeared to be approaching steady state concentrations as phenol was irradiated in the model. The nonlinear model for imaginary refractive index did not significantly over predict the imaginary refractive index for phenol.

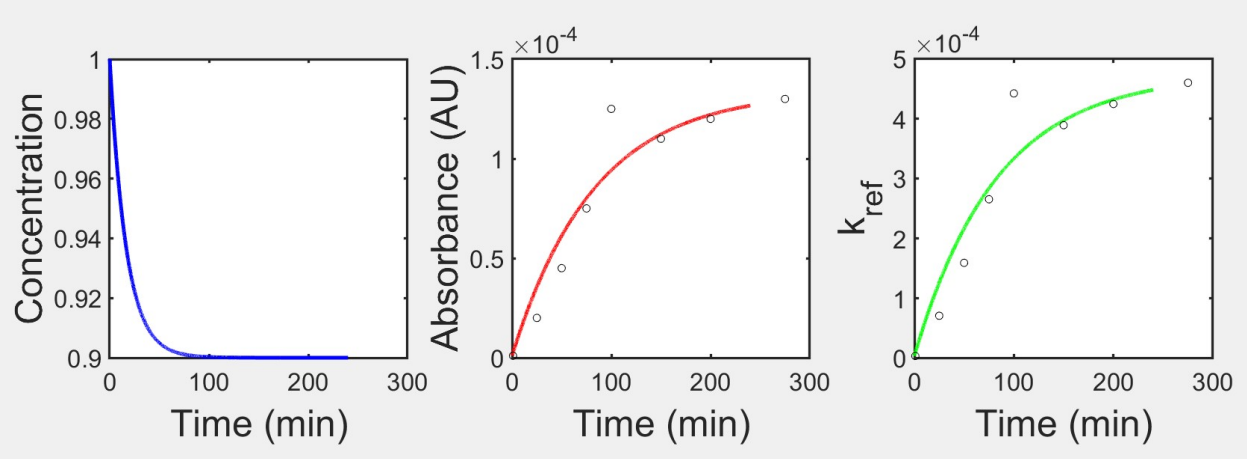

Figure 14: *Kinetic model for guaiacol*

The nonlinear model of imaginary refractive index for guaiacol predicted most of the experimental data, except one outlier. Guaiacol reaches steady state at approximately 100 minutes when the imaginary refractive index begins to decrease.

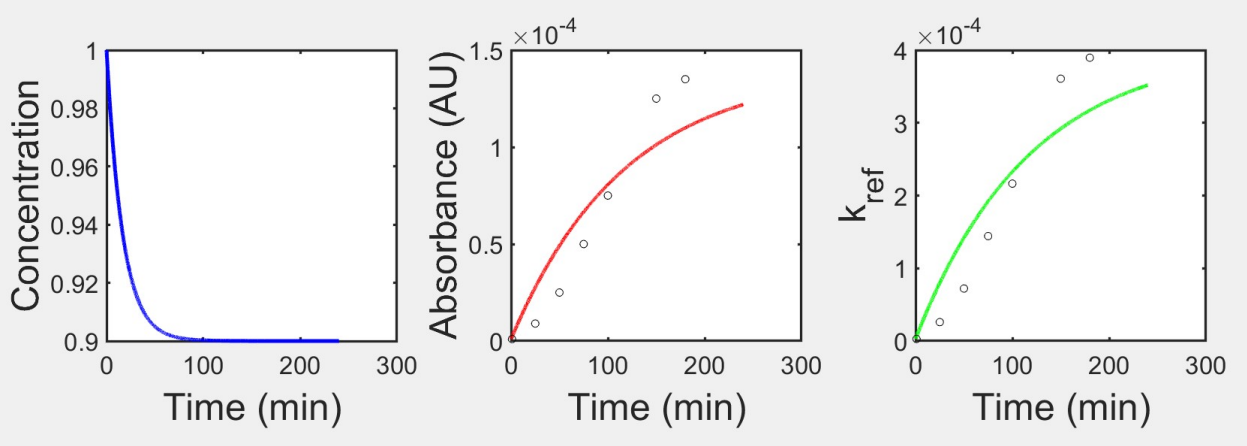

Figure 15: *Kinetic model for vanillin*

The nonlinear model for vanillin overpredicted imaginary refractive index until approximately 100 minutes. At 100 minutes, the nonlinear model significantly underpredicts the imaginary refractive index for vanillin. Vanillin does not reach a clear steady state or maximum absorbance.

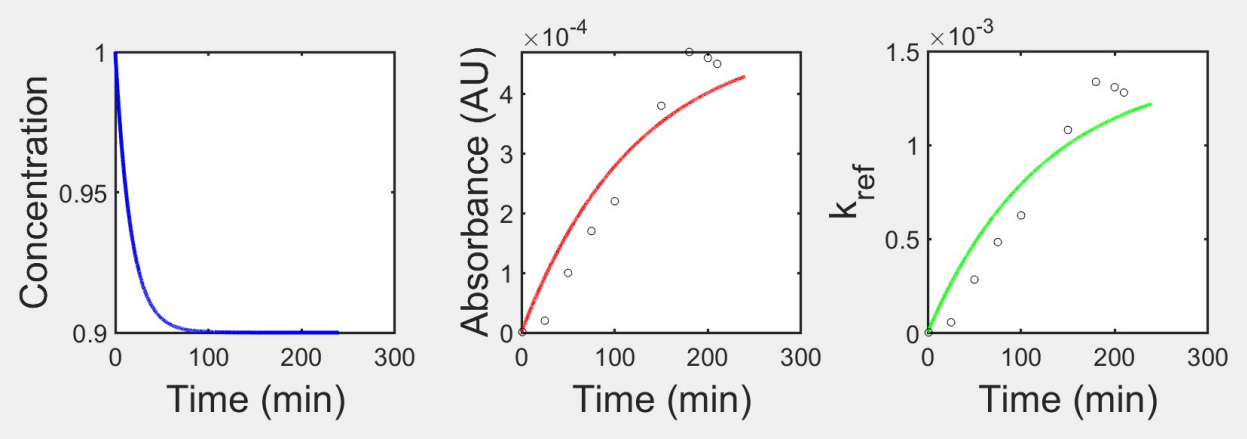

Figure 16: *Kinetic model for syringol*

The kinetic model for syringol follows the experimental results for imaginary refractive index until approximately 175 minutes. At 175 minutes, the model underpredicts the imaginary refractive index for syringol. Syringol does not reach a clear steady state.

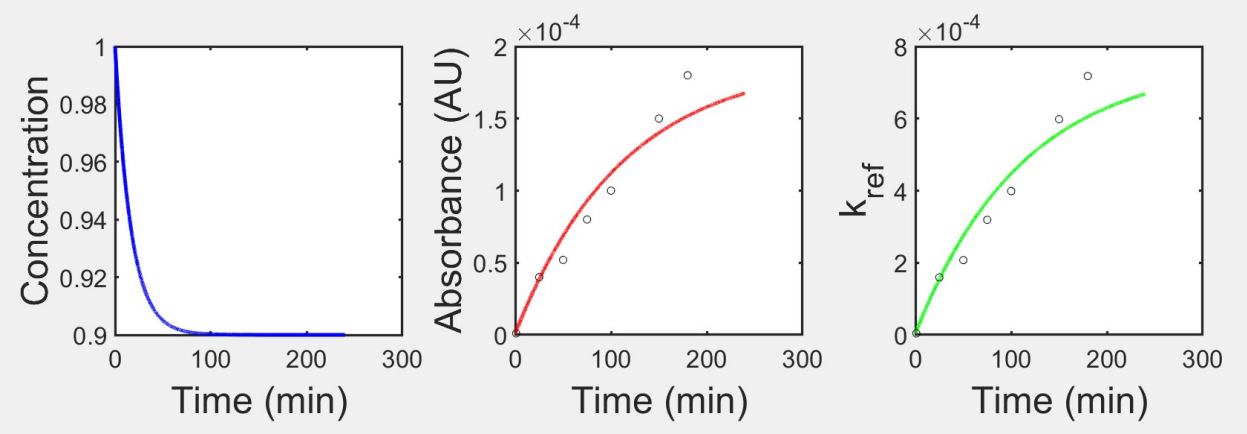

Figure 17: *Kinetic model for catechol*

The kinetic model for catechol does not predict the imaginary refractive index with a nonlinear trend. The model underpredicts imaginary refractive index at

approximately 150 minutes. Catechol does not reach maximum absorbance or steady state.

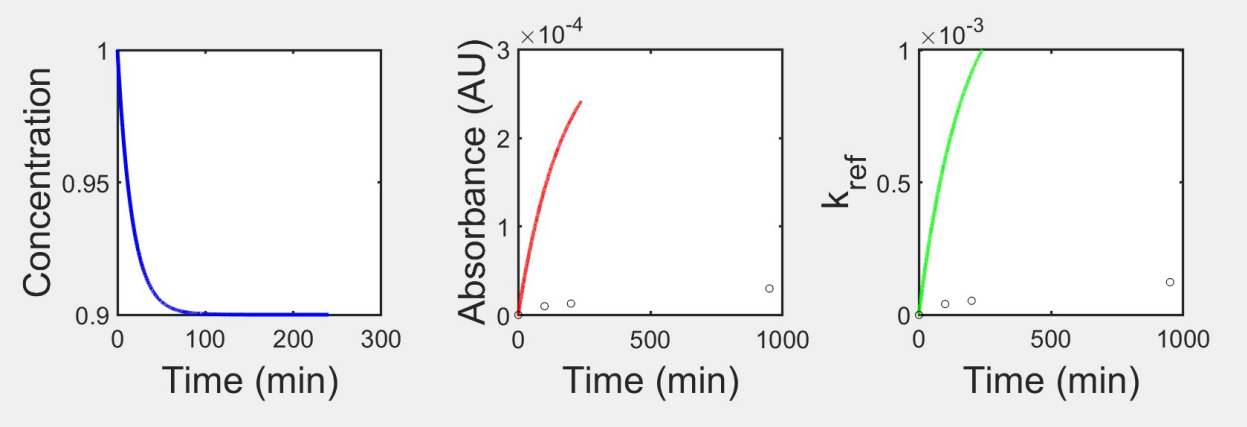

Figure 18: *Kinetic model for benzaldehyde*

The kinetic model for benzaldehyde significantly overpredicted absorbance and imaginary refractive index. Benzaldehyde does not reach a clear steady state or maximum absorbance, even with a time scale of 1000 minutes.

3.4. Error results

The standard error for the linear and nonlinear models were calculated and can be found in Table 3 and Table 4 below.

Table 3: *Linear and nonlinear model standard error for first 6 compounds*

Compound	phenol	p-hydroxybenzaldehyde	guaiacol	vanillin	syringol	4-methylsyringol
Linear Standard Error for k (%)	1.89	7.92	29.0	6.31	24.5	6.31
Nonlinear Standard Error for A (%)	3.48	8.23	5.18	8.12	12.1	2.80

Table 4: *Linear and nonlinear model standard error for second 6 compounds*

Compound	syringaldehyde	pyrogallol	catechol	resorcinol	3,4-dimethoxy-benzaldehyde	benzaldehyde
Linear Standard Error for k (%)	3.17	103	6.36	44.5	0.909	5.54
Nonlinear Standard Error for A (%)	7.10	6.53	5.33	5.32	2.74	13.5

In addition, the standard error of the kinetic models for 6 compounds was calculated and can be found in Table 5 below.

Table 5: *Standard error for kinetic models for 6 compounds*

Compound	phenol	guaiacol	vanillin	syringol	catechol	benzaldehyde
Standard Error (%)	84.2	52.9	41.9	46.8	41.9	281.7

4. Discussion

The limited data derived from experimental measurements of absorbance over time under irradiance contributes to uncertainty surrounding the accuracy of these models. Even so, all three models demonstrated potential for predicting the imaginary refractive index based on certain assumptions and compound rate constants. Therefore, the models establish a general model for predicting and quantifying the absorbing and warming component of BB emission compounds.

4.1. Linear fitting of imaginary refractive indices with absorbance values

The linear model for predicting imaginary refractive index was shown to predict imaginary refractive index for phenol, p-hydroxybenzaldehyde, vanillin, catechol, and 3,4-methoxybenzaldehyde. The differing alignments could be due to a multitude of factors including the time for each compound to completely react. In addition, certain compounds may have short-term kinetics in which the compound forms colored compounds quickly and the absorbance stabilizes at a certain time.

This study found that certain compounds have a unique maximum absorbance and reaction time. Certain compounds react quicker and create colored compounds at a significantly faster rate. Furthermore, the compounds that followed the linear model may follow first order reaction kinetics, while compounds that followed the nonlinear model may follow second order reaction kinetics.

Phenol followed the linear trend for imaginary refractive index and did not appear to reach steady state concentrations. Phenol may require longer reaction times under irradiation to reach steady-state. Even so, the phenol measurements only used

four data points so more data is necessary to understand the short and long term kinetics of phenol. Catechol did not appear to reach a steady-state concentration. This could demonstrate that catechol requires a longer reaction times for complete photodegradation than the given time. Pyrogallol did not follow the linear trend for imaginary refractive index. Pyrogallol reaches steady-state levels at approximately 75 minutes. After this point, the imaginary refractive index, and therefore the absorbance, does not change significantly. As a result, pyrogallol kinetics may have more impact during short term reactions. Guaiacol reaches steady-state levels for imaginary refractive index at approximately 100 minutes. Guaiacol imaginary refractive index did not follow a linear trend. The photochemical reactions of guaiacol and absorbing products may not change after long periods of time. Therefore, the shorter term kinetics are more important for guaiacol.

Overall, compounds did not appear to follow an overall linear trend. However, compounds may follow a linear trend before maximum absorbance and steady-state is reached. Certain compounds, such as phenol, did not reach steady-state and may require a longer reaction time to reach maximum absorbance. Compounds such as pyrogallol and guaiacol reached steady-state at different maximum absorbances before two hours of reaction time. These compounds may not require a long reaction time to reach maximum absorbance. A linear model of the kinetics leading up to steady-state could be created to determine whether compounds follow linear trends before reaching maximum absorbance.

4.2. Nonlinear modeling of absorbance

Although the nonlinear model for absorbance appeared to work for phenol, steady-state is not strongly demonstrated and longer times are necessary to identify when maximum absorbance is reached. Phenol kinetics also worked for linear fitting. Therefore, further experimental data is needed and should include absorbance changes for longer reaction times. Syringol did not appear to follow the nonlinear model for absorbance, fitting the time constant. Syringol reaches steady-state at approximately 180 minutes. The experimental absorbance for syringol may vary from the nonlinear model because the absorbance changes before reaching maximum absorbance appear to be linear. 4-methylsyringol did not follow all experimental data points with the nonlinear model for absorbance. Although 4-methylsyringol appears to reach steady state at around 150 minutes, the kinetics leading up to steady state do not match the nonlinear fit. Syringaldehyde did not follow the nonlinear fit for absorbance. Syringaldehyde does not reach a clear steady state. The experimental absorbance measurements stop at around 375 minutes. Syringaldehyde may require long reaction periods to reach maximum absorbance.

The nonlinear model for absorbance worked for phenol, p-hydroxybenzaldehyde, guaiacol, catechol, and resorcinol. The nonlinear model fit experimental results for compounds that reached a clear steady state concentration. For benzaldehyde, the fit was significantly improved when the initial concentration was changed from 10 AU to 100 AU. This could have resulted because the *lsqcurvefit* function finds the local minimum for error instead of the global minimum.

4.3. Kinetic model

The imaginary refractive index for guaiacol followed the nonlinear model and reaches steady state at around 100 minutes. Besides one outlier, the nonlinear fit for imaginary refractive index aligns with the experimental data. The nonlinear model for imaginary refractive index did not follow the experimental data for vanillin. Vanillin does not appear to reach steady state in the time scale. Syringol did not follow the nonlinear model for imaginary refractive index closely. Although the imaginary refractive index for syringol begins decreasing at approximately 175 minutes, a clear steady state is not reached. The kinetic model did not fit catechol experimental measurements because steady state is not reached. The kinetic model for benzaldehyde varied significantly from the experimental data. This could have been due to an incorrect time constant.

The coupled models varied from the experimental data. This could be due to initial concentration differences between the model and the experimental data. Furthermore, the estimations for the time constant may differ from the actual constant. The scaled difference between the model and experimental data was approximated.

Limitations to this study includes the size of the data set. The Chang and Thompson data only represents 12 compounds and there are as many different major primary compounds emitted from BB. In addition, future experimental measurements of absorbance of the compounds could be used to create a more robust data set for inputs into the model.

5. Future Work

The initial research plan included experimental measurements of absorbance for three BB emission proxies. Complications with laboratory access (due to COVID-19) and electrical issues with the solar simulator resulted in an inability to obtain experimental absorbance measurements. As a result, a substantial amount of future work is available to verify the numerical models created in this study. Although the actual experimentation was not performed in this study, a detailed methodology was created, in addition to the construction of a darkroom necessary for the experiment. The following sections outline the proposed experimental methodology.

5.1. Solar Simulator

A solar simulator is a device that mimics the irradiation of the sun in a laboratory setting. In this experiment, the solar simulator will allow the test compounds to be irradiated with similar conditions that would exist in the atmosphere. In this controlled setting, compounds can undergo irradiation while the kinetics and absorbance changes can be observed and measured easily with accessible instruments in the laboratory.

5.2. Ferrioxalate actinometry

Chemical actinometry is a commonly used method for quantifying photochemical properties such as irradiance and photolysis rates (Laszakovits et al., 2017). Chemical actinometry can be used to calculate irradiance by experimentally determining the reaction rate of a chemical actinometer and using the solution's known properties of quantum yield and absorption (Laszakovits et al., 2017).

Ferrioxalate is a well-established chemical actinometer in which potassium ferrioxalate degrades under irradiation by UV and visible light (Montalti et al., 2006). Experimental processes that use ferrioxalate must be conducted in a dark space to avoid degradation of ferrioxalate in natural light. In addition, ferrioxalate contains iron complexes that can produce free radical species and oxidize a variety of organic compounds (Kocar & Inskeep, 2003). Therefore, reaction vessels used in ferrioxalate actinometry calibration must be used separately from experimental reaction vessels to prevent oxidation. Oxidation can cause reactions that are not part of the actual experiment and the resulting data could be affected.

5.3. Darkroom construction

A darkroom is an important structure that can be used for photosensitive experiments to prevent external influence from light sources. Due to the photosensitivity of ferrioxalate, a portable darkroom is required to calibrate the solar simulator using ferrioxalate as a chemical actinometer. The darkroom was constructed out of lightweight foam insulation boards that were cut into three large panels for the left, right, and top of the darkroom structure. Each board was cut to fit the specific dimensions of the laboratory room setup. The top board was cut to fit securely on the left and right boards. A blackout curtain was used to block light from entering the back of the darkroom and allow easy access from the darkroom.

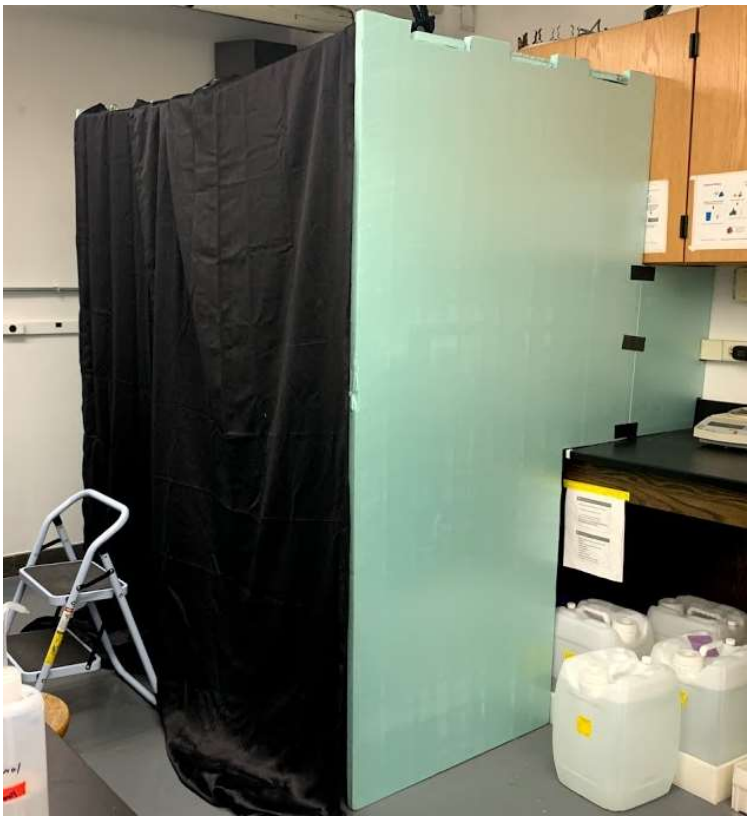

Figure 3: *Constructed darkroom*

5.4. Solar simulator calibration

First, the ferrioxalate actinometer will be prepared. A 500 mL, 0.05 M sulfuric acid stock was made using 1.33 mL of pure sulfuric acid and 498.67 mL of deionized water. In a darkroom, 0.012 M Ferrioxalate stock solution will be made by adding 3 g of potassium ferrioxalate to 500 mL of 0.05 M sulfuric acid in a beaker (Montalti et al., 2006). The solution will be covered with foil and kept in a dark storage room.

Next, the colorimeter reagent will be prepared. 13.33 mL of pure sulfuric acid will be added to 486.67 mL of deionized water (DI) to make 500 mL 0.5 M sulfuric acid stock solution. Then, 112.5 g of sodium acetate and 0.5 g of phenanthroline will be

added to 500 mL of 0.5 M sulfuric acid. This solution will be stored in the dark to prevent photodecomposition.

Calibration will be conducted inside a darkroom. First, the solar simulator will be turned on and warmed up for about 15 minutes. Four 3.5 mL cuvettes will be labeled for 0 minutes, 15 minutes, 30 minutes, and 1 hour time points. Inside the darkroom, 3.2 mL of ferrioxalate actinometer will be added to four 3.5 mL cuvette and placed in the solar simulator. 0.1 mL samples will be removed at the different time points and mixed with 3.2 mL of colorimetric solution. The samples will be kept in the dark for about 30 minutes. Next, a UV-Vis spectrometer will be used to measure the absorbance of the samples at 510 nm. Then, a plot will be created for Absorbance (510 nm) vs Time (s). The slope of this line will be used to convert absorbance to irradiance or light intensity using the following equation:

$$E^0 = \frac{k * V_{diluted} * L}{1000 * \in_{510} * \emptyset * V_{subsample}}$$

Equation 7: *The rate of absorbance (k) can be converted to irradiance (E^0) with the volume of diluted subsample ($V_{diluted}$), path length (L), extinction coefficient ($\in_{510}$), quantum yield ($\emptyset$), volume of the subsample ($V_{subsample}$), and a dilution factor of 1000.*

5.5. Organic solution experiments

Eight total experiments will be performed in triplicate:

- Phenol
- Benzaldehyde
- Furfural
- Hydrogen peroxide and phenol
- Hydrogen peroxide and benzaldehyde
- Hydrogen peroxide and furfural
- Deionized water

For each experiment, 3.3 mL of the test compound and a buffer with a pH of 5 will be added to four different cuvettes. The solar simulator was turned on to warm up for about 15 minutes. The cuvettes were placed in the solar simulator and removed at 0, 15, 30, and 45 minutes for short term kinetic experiments. For longer kinetic experiments, the cuvettes were removed at 0, 1 hour, 2 hours, and 3 hours.

A UV-Vis spectrometer will be used to measure the absorbance of subsamples at various wavelengths (200-700 nm).Then, a plot with Absorbance (200-700 nm) vs Time (s) was created. Then, the imaginary refractive index (k) was calculated.

6. Conclusion

6.1. Added value of study

This study established potential for quantifying radiative forcing of biomass burning emissions and understanding climate impacts. These models also modeled the chemical differences between compounds under irradiation, shown by different absorbance kinetics and varying reaction time requirements. The compounds that had not reached steady state and maximum absorbance followed the linear model for

imaginary refractive indices. The compounds that reached steady state and maximum absorbance fit the nonlinear models for absorbance and imaginary refractive indices. Compounds reached steady state and maximum absorbance at varying times, ranging from 1 hour to over 2.5 hours. Some compounds did not reach steady state or maximum absorbance in the experimental time frame so the reaction times are undetermined. Therefore, the experimental methods for absorbance measurements under irradiation are an important next step to determine the maximum absorbance and imaginary refractive indices of compounds with longer kinetics. The experimental methods and code created in this study will guide future work in verifying and adapting the models.

6.2. Implications

The imaginary refractive indices modeled in this study can be input into developed code to quantify the radiative forcing and climate change impacts of the compounds. This information can be used to contribute atmospheric chemistry knowledge to improve and progress understandings of BB impacts to climate change. This study also created a framework for future work that can continue to implement and improve kinetic modeling of BB emission interactions with light and their warming effects. As a result, uncertainties surrounding BB impacts to climate change will be reduced.

7. References

Bohren, C. F., & Huffman, D. R. (1998). *Absorption and Scattering of Light by Small Particles*. Wiley. https://doi.org/10.1002/9783527618156

Cappa, C. D., Onasch, T. B., Massoli, P., Worsnop, D. R., Bates, T. S., Cross, E. S., Davidovits, P., Hakala, J., Hayden, K. L., Jobson, B. T., Kolesar, K. R., Lack, D. A., Lerner, B. M., Li, S. M., Mellon, D., Nuaaman, I., Olfert, J. S., Petäjä, T., Quinn, P. K., … Zaveri, R. A. (2012). Radiative absorption enhancements due to the mixing state of atmospheric black carbon. *Science*, *337*(6098), 1078–1081. https://doi.org/10.1126/science.1223447

Chang, J. L., & Thompson, J. E. (2010). Characterization of colored products formed during irradiation of aqueous solutions containing H2O2 and phenolic compounds. *Atmospheric Environment*, *44*(4), 541–551. https://doi.org/10.1016/j.atmosenv.2009.10.042

Chylek, P., Lee, J. E., Romonosky, D. E., Gallo, F., Lou, S., Shrivastava, M., Carrico, C. M., Aiken, A. C., & Dubey, M. K. (2019). Mie Scattering Captures Observed Optical Properties of Ambient Biomass Burning Plumes Assuming Uniform Black, Brown, and Organic Carbon Mixtures. *Journal of Geophysical Research: Atmospheres*, *124*(21), 11406–11427. https://doi.org/10.1029/2019JD031224

Dahlkötter, F., Gysel, M., Sauer, D., Minikin, A., Baumann, R., Seifert, P., Ansmann, A., Fromm, M., Voigt, C., & Weinzierl, B. (2014). The Pagami Creek smoke plume after long-range transport to the upper troposphere over Europe – Aerosol properties and black carbon mixing state. *Atmospheric Chemistry and Physics*,

14(12), 6111–6137. https://doi.org/10.5194/acp-14-6111-2014

Duarte, R. M. B. O., Santos, E. B. H., Pio, C. A., & Duarte, A. C. (2007). Comparison of structural features of water-soluble organic matter from atmospheric aerosols with those of aquatic humic substances. *Atmospheric Environment*, *41*(37), 8100–8113. https://doi.org/10.1016/j.atmosenv.2007.06.034

Fan, X., Zheng, W., & Singh, D. J. (2014). Light scattering and surface plasmons on small spherical particles. *Light: Science & Applications*, *3*(6), e179–e179. https://doi.org/10.1038/lsa.2014.60

Hatch, L. E., Luo, W., Pankow, J. F., Yokelson, R. J., Stockwell, C. E., & Barsanti, K. C. (2015). Identification and quantification of gaseous organic compounds emitted from biomass burning using two-dimensional gas chromatography-time-of-flight mass spectrometry. *Atmospheric Chemistry and Physics*. https://doi.org/10.5194/acp-15-1865-2015

Hennigan, C. J., Miracolo, M. A., Engelhart, G. J., May, A. A., Presto, A. A., Lee, T., Sullivan, A. P., McMeeking, G. R., Coe, H., Wold, C. E., Hao, W. M., Gilman, J. B., Kuster, W. C., De Gouw, J., Schichtel, B. A., Collett, J. L., Kreidenweis, S. M., & Robinson, A. L. (2011). Chemical and physical transformations of organic aerosol from the photo-oxidation of open biomass burning emissions in an environmental chamber. *Atmospheric Chemistry and Physics*, *11*(15), 7669–7686. https://doi.org/10.5194/acp-11-7669-2011

Jimenez, J. L., Canagaratna, M. R., Donahue, N. M., Prevot, A. S. H., Zhang, Q., Kroll, J. H., DeCarlo, P. F., Allan, J. D., Coe, H., Ng, N. L., Aiken, A. C., Docherty, K. S.,

Ulbrich, I. M., Grieshop, A. P., Robinson, A. L., Duplissy, J., Smith, J. D., Wilson, K. R., Lanz, V. A., … Worsnop, D. R. (2009). Evolution of organic aerosols in the atmosphere. *Science*, *326*(5959), 1525–1529. https://doi.org/10.1126/science.1180353

Kocar, B. D., & Inskeep, W. P. (2003). Photochemical oxidation of As(III) in ferrioxalate solutions. *Environmental Science and Technology*. https://doi.org/10.1021/es020939f

Laskin, A., Laskin, J., & Nizkorodov, S. A. (2015). Chemistry of Atmospheric Brown Carbon. In *Chemical Reviews*. https://doi.org/10.1021/cr5006167

Laszakovits, J. R., Berg, S. M., Anderson, B. G., O'Brien, J. E., Wammer, K. H., & Sharpless, C. M. (2017). P-Nitroanisole/pyridine and p-Nitroacetophenone/pyridine actinometers revisited: Quantum yield in comparison to ferrioxalate. *Environmental Science and Technology Letters*, *4*(1), 11–14. https://doi.org/10.1021/acs.estlett.6b00422

Lee, H. J., Aiona, P. K., Laskin, A., Laskin, J., & Nizkorodov, S. A. (2014). Effect of solar radiation on the optical properties and molecular composition of laboratory proxies of atmospheric brown carbon. *Environmental Science and Technology*. https://doi.org/10.1021/es502515r

Liu, P. F., Abdelmalki, N., Hung, H. M., Wang, Y., Brune, W. H., & Martin, S. T. (2015). Ultraviolet and visible complex refractive indices of secondary organic material produced by photooxidation of the aromatic compounds toluene and m-xylene. *Atmospheric Chemistry and Physics*, *15*(3), 1435–1446.

https://doi.org/10.5194/acp-15-1435-2015

Montalti, M., Credi, A., Prodi, L., & Gandolfi, M. T. (2006). Handbook of Third Edition. In *Handbook of Third Edition*.

Seinfeld, J. H., & Pandis, and S. N. (2016). *Atmospheric Chemistry and Physics* (3rd ed.). John Wiley & Sons, Incorporated.

Shrivastava, M., Cappa, C. D., Fan, J., Goldstein, A. H., Guenther, A. B., Jimenez, J. L., Kuang, C., Laskin, A., Martin, S. T., Ng, N. L., Petaja, T., Pierce, J. R., Rasch, P. J., Roldin, P., Seinfeld, J. H., Shilling, J., Smith, J. N., Thornton, J. A., Volkamer, R., … Zhang, Q. (2017). Recent advances in understanding secondary organic aerosol: Implications for global climate forcing. *Reviews of Geophysics*. https://doi.org/10.1002/2016RG000540

Smith, J. D., Kinney, H., & Anastasio, C. (2016). Phenolic carbonyls undergo rapid aqueous photodegradation to form low-volatility, light-absorbing products. *Atmospheric Environment*, *126*, 36–44. https://doi.org/10.1016/j.atmosenv.2015.11.035

Sun, H., Biedermann, L., & Bond, T. C. (2007). Color of brown carbon: A model for ultraviolet and visible light absorption by organic carbon aerosol. *Geophysical Research Letters*, *34*(17), 1–5. https://doi.org/10.1029/2007GL029797

Tuet, W. Y., Chen, Y., Xu, L., Fok, S., Gao, D., Weber, R. J., & Ng, N. L. (2017). Chemical oxidative potential of secondary organic aerosol (SOA) generated from the photooxidation of biogenic and anthropogenic volatile organic compounds. *Atmospheric Chemistry and Physics*, *17*(2), 839–853.

https://doi.org/10.5194/acp-17-839-2017

Zhang, Q., Jimenez, J. L., Canagaratna, M. R., Allan, J. D., Coe, H., Ulbrich, I., Alfarra, M. R., Takami, A., Middlebrook, A. M., Sun, Y. L., Dzepina, K., Dunlea, E., Docherty, K., DeCarlo, P. F., Salcedo, D., Onasch, T., Jayne, J. T., Miyoshi, T., Shimono, A., … Worsnop, D. R. (2007). Ubiquity and dominance of oxygenated species in organic aerosols in anthropogenically-influenced Northern Hemisphere midlatitudes. *Geophysical Research Letters*, *34*(13), n/a-n/a. https://doi.org/10.1029/2007GL029979

Appendix 1

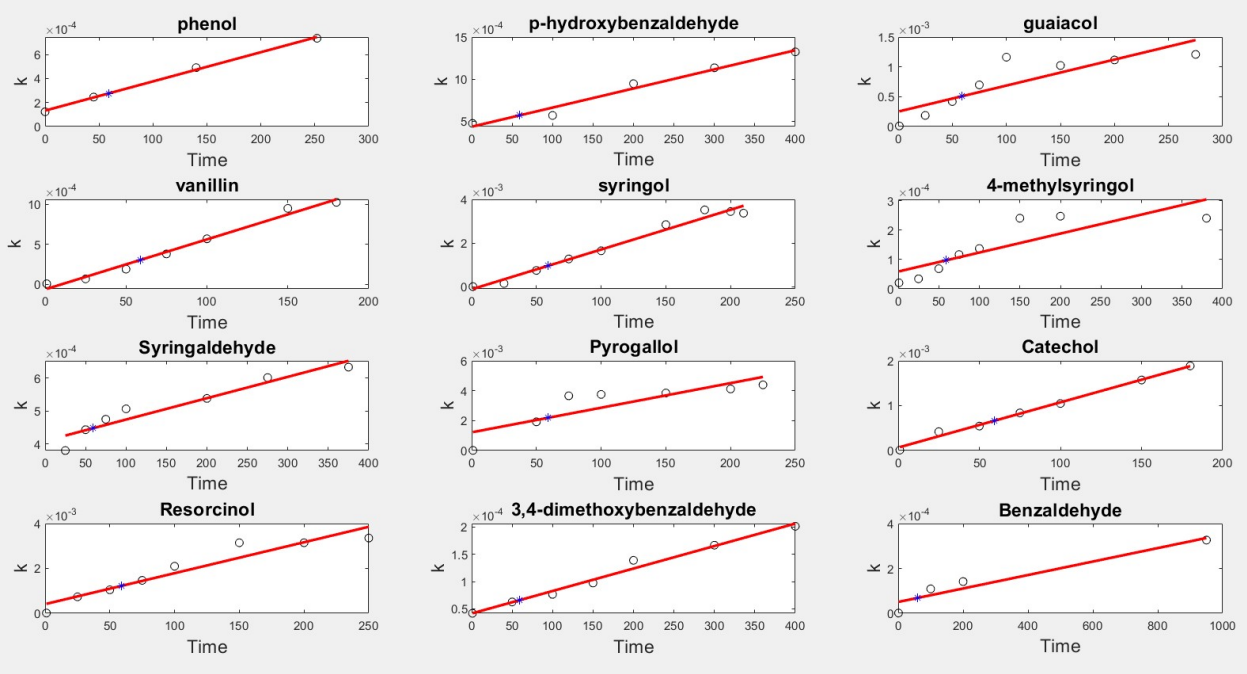

Figure 1a: *Linear models for 12 compounds*

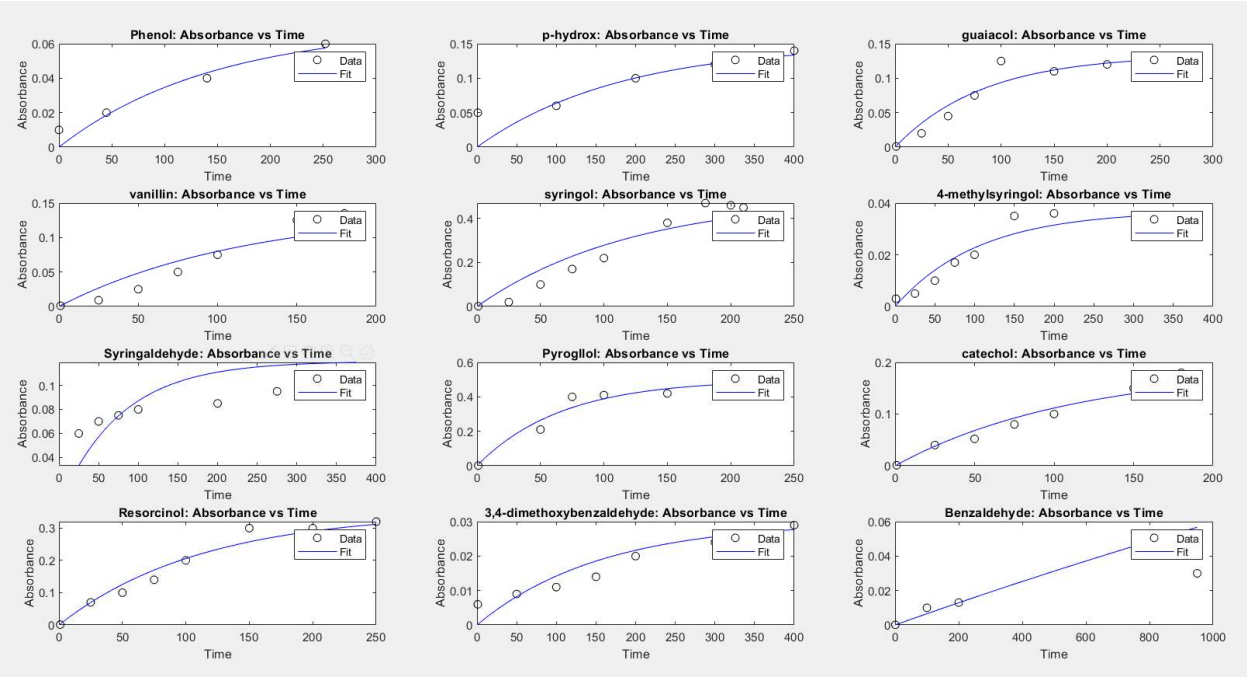

Figure 1b: *Nonlinear models for 12 compounds*

Appendix 2a

Linear fitting of imaginary refractive indices with absorbance values

```
% Fitting Refractive index (k) using MW of compounds
% Refractive_Index_MW.m
% Inputs: Absorbance and Time from Chang & Thompson

clc
clear
close all

%% Absorbance and time data

% Phenol

xdata{1} = [0.01 45 140 252]; %time

% p-hydroxybenzaldehyde

xdata{2} = [1 100 200 300 400]; %time

% guaiacol

xdata{3} = [1 25 50 75 100 150 200 275]; %time

% vanillin

xdata{4} = [1 25 50 75 100 150 180]; %time

% syringol

xdata{5} = [1 25 50 75 100 150 180 200 210]; %time

% 4-methylsyringol

xdata{6} = [1 25 50 75 100 150 200 380]; %time

% Syringaldehyde

xdata{7} = [25 50 75 100 200 275 375]; %time

% Pyrogallol
```

```
xdata{8} = [1 50 75 100 150 200 225]; %time

% Catechol

xdata{9} = [1 25 50 75 100 150 180]; %time

% Resorcinol

xdata{10} = [1 25 50 75 100 150 200 250]; %time

% 3,4-dimethoxybenzaldehyde

xdata{11} = [1 50 100 150 200 300 400]; %time

% Benzaldehyde

xdata{12} = [1 100 200 950]; %time

% Absorbance

% Phenol

ydata{1} = [0.01 0.02 0.04 0.06]; % absorbance
molw(1) = 94.11; % molecular weight g/mol

% p-hydroxybenzaldehyde

ydata{2} = [0.05 0.06 0.1 0.12 0.14]; % absorbance
molw(2) = 122.1213;

% guaiacol

ydata{3} = [0.001 0.02 0.045 0.075 0.125 0.11 0.12 0.13]; %
absorbance
molw(3) = 124.14;

% vanillin

ydata{4} = [0.001 0.009 0.025 0.05 0.075 0.125 0.135]; %
absorbance
molw(4) = 152.15;

% syringol
```

```
ydata{5} = [0.001 0.02 0.1 0.17 0.22 0.38 0.47 0.46
0.45]; % absorbance
molw(5) = 154.16;

% 4-methylsyringol

ydata{6} = [0.003 0.005 0.01 0.017 0.02 0.035 0.036
0.035]; % absorbance
molw(6) = 168.19;

% Syringaldehyde

ydata{7} = [0.06 0.07 0.075 0.08 0.085 0.095 0.1]; %
absorbance
molw(7) = 182.17;

% Pyrogallol

ydata{8} = [0.001 0.21 0.4 0.41 0.42 0.45 0.48]; %
absorbance
molw(8) = 126.11;

% Catechol

ydata{9} = [0.001 0.04 0.052 0.08 0.1 0.15 0.18]; %
absorbance
molw(9) = 110.1;

% Resorcinol

ydata{10} = [0.001 0.07 0.1 0.14 0.2 0.3 0.3 0.32]; %
absorbance
molw(10) = 110.1;

% 3,4-dimethoxybenzaldehyde

ydata{11} = [0.006 0.009 0.011 0.014 0.02 0.024 0.029]; %
absorbance
molw(11) = 166.17;

% Benzaldehyde

ydata{12} = [0.0001 0.01 0.013 0.03]; % absorbance
molw(12) = 106.124;
```

```
%% Assumptions

A = ydata; % absorbance
time = xdata;
L = 0.01; % assume optical path length (m)
p = 1.4*10^3; % assume material density (kg m^-3)
w = 450*10^-9; % assume wavelength

%% Calculate the experimental 'k' for each compound based
on Abs and conc
for j=1:12
    for z=1:length(A{j})
        c = conc(molw(j));
        k{j}(z) =
(( log(10)/(4*pi) )*( (p*w)/(c*L) ))*(A{j}(z));
    end
end

%% Plot the experimental 'k' vs time

Name = {'phenol' 'p-hydroxybenzaldehyde' 'guaiacol'
'vanillin' 'syringol' '4-methylsyringol' 'Syringaldehyde'
'Pyrogallol' 'Catechol' 'Resorcinol' '3,4-
dimethoxybenzaldehyde' 'Benzaldehyde'};

figure('Name','Absorbance vs k')

% for i=1:12
%     subplot(4,3,i)
%     plot(A{i},k{i},'k.')
%     title(Name{i})
%     xlabel('Absorbance')
%     ylabel('k')
% end

%% Plot experimental 'k' vs time and fitting results

% figure('Name','k vs time') % *** uncommment for single
graph

for i=1:12

    figure(i) % individual plots *** comment for signle
graph
```

```
    % subplot(4,3,i) % *** uncomment for single graph
    plot(time{i},k{i},'ko')
    % Plot experimental data

    coefficients = polyfit(time{i}, k{i}, 1);
    % Returns coefficients for polynomial 'p(time)' of
degree
    % '1' that is the best fit (least-squares) for data in
'k'
    % *Source: MATLAB help file*

    xFit{i} = linspace(min(time{i}), max(time{i}), 1000);
    % Generates '1000' points for 'time'
    % The spacing between the points is (max-min)/(1000-1)

    yFit{i} = polyval(coefficients , xFit{i}); % k
    % Evaluates the polynomial 'coefficients' at each point
    % in 'xFit', The argument 'coefficients' is a vector of
length n+1
    % whose elements are the coefficients (in descending
powers of an nth
    % degree polynomial.

    hold on;
    plot(xFit{i}, yFit{i}, 'r-', 'LineWidth', 2);
    % grid on;
    title(Name{i},'FontSize',14)
    xlabel('Time','FontSize',14)
    ylabel('k','FontSize',14)
    in = find(xFit{i}<61 & xFit{i}>59,1);
    % find index of time at 60 min
    one_hr(i) = yFit{i}(in(1));
    % k at 60 min
    plot(xFit{i}(in),one_hr(i),'b*')

end

global kForEach

kForEach{1} = Name;
kForEach{2} = one_hr;

% Model value of k for each time, calculate R2 (error)
```

```
% for w = 1:12
%     res = 0;
%         for v = 1:length(xdata{w})
%             k_mod_i = find(xFit{w}==xdata{w}(v)); % index
of k
%             k_mod = yFit{w}(k_mod_i);
%             k_exp = k{w}(v);
%         end
%     res_sum{w} = res;
% end

% average

for i=1:12
    avg(i) = mean(k{i});
end

avg

function cc = conc(mw)
% Calculates concentration in kg/m^3 given a molecular
weight

    uM = 10000; % uM per M
    ml = 1000; % mL per L
    cc = (uM/ml)*(10^6)*mw*(10^-9); % Conversions

end
```

Appendix 2b

Nonlinear modeling of absorbance

```
%% Fitting Absorbance using absorbance data from Chang &
Thompson

clc
clear
close all

%% Phenol

xdata = [0.01 45 140 252]; % time
ydata = [0.01 0.02 0.04 0.06]; % absorbance
x0 = [10]; % initial time
Amax = 0.07; % initial absorbance

% Function to calculate absorbance
fun = @(x,xdata)Amax*(1-exp(-xdata/x));
% Nonlinear curve fitting starts at 'x0' and finds
coefficients 'x' to fit
% the nonlinear function 'fun(x, xdata)' to 'ydata'.
[x,resnorm,residual,exitflag,output] =
lsqcurvefit(fun,x0,xdata,ydata);

% Creates a linearly spaced time vector the size of xdata
times = linspace(xdata(1),xdata(end));

figure('Name','Phenol')
plot(xdata,ydata,'ko',times,fun(x,times),'b-')
legend('Data','Fit')
title('Phenol: Absorbance vs Time')
xlabel('Time')
ylabel('Absorbance')

% p-hydroxybenzaldehyde

xdata = [1 24 25 50 75 90 100 150 220]; %time
ydata = [0.01 0.09 0.1 0.24 0.36 0.4 0.45 0.451 0.46]; %
absorbance
x0 = [10]; % initial value
Amax = 0.47;
```

```
fun = @(x,xdata)Amax*(1-exp(-xdata/x)); % function
[x,resnorm,residual,exitflag,output] =
lsqcurvefit(fun,x0,xdata,ydata);

times = linspace(xdata(1),xdata(end));

figure('Name','p-hydroxybenzaldehyde')
plot(xdata,ydata,'ko',times,fun(x,times),'b-')
legend('Data','Fit')
title('p-hydrox: Absorbance vs Time')
xlabel('Time')
ylabel('Absorbance')

% guaiacol

xdata = [1 25 50 75 100 150 200 275]; %time
ydata = [0.001 0.02 0.045 0.075 0.125 0.11 0.12 0.13]; %
absorbance
x0 = [10]; % initial value
Amax = 0.134;

fun = @(x,xdata)Amax*(1-exp(-xdata/x)); % function
[x,resnorm,residual,exitflag,output] =
lsqcurvefit(fun,x0,xdata,ydata);

times = linspace(xdata(1),xdata(end));

figure('Name','guaiacol')
plot(xdata,ydata,'ko',times,fun(x,times),'b-')
legend('Data','Fit')
title('guaiacol: Absorbance vs Time')
xlabel('Time')
ylabel('Absorbance')

% vanillin

xdata = [1 25 50 75 100 150 180]; %time
ydata = [0.001 0.009 0.025 0.05 0.075 0.125 0.135]; %
absorbance
x0 = [10]; % initial value
Amax = 0.14;

fun = @(x,xdata)Amax*(1-exp(-xdata/x)); % function
```

```
[x,resnorm,residual,exitflag,output] =
lsqcurvefit(fun,x0,xdata,ydata);

times = linspace(xdata(1),xdata(end));

figure('Name','vanillin')
plot(xdata,ydata,'ko',times,fun(x,times),'b-')
legend('Data','Fit')
title('vanillin: Absorbance vs Time')
xlabel('Time')
ylabel('Absorbance')

% syringol

xdata = [1 25 50 75 100 150 180 200 210]; %time
ydata = [0.001 0.02 0.1 0.17 0.22 0.38 0.47 0.46 0.45]; %
absorbance
x0 = [10]; % initial value
Amax = 0.5;

fun = @(x,xdata)Amax*(1-exp(-xdata/x)); % function
[x,resnorm,residual,exitflag,output] =
lsqcurvefit(fun,x0,xdata,ydata);

times = linspace(xdata(1),xdata(end));

figure('Name','syringol')
plot(xdata,ydata,'ko',times,fun(x,times),'b-')
legend('Data','Fit')
title('syringol: Absorbance vs Time')
xlabel('Time')
ylabel('Absorbance')

% 4-methylsyringol

xdata = [1 25 50 75 100 150 200 380]; %time
ydata = [0.003 0.005 0.01 0.017 0.02 0.035 0.036 0.035]; %
absorbance
x0 = [10]; % initial value
Amax = 0.037;

fun = @(x,xdata)Amax*(1-exp(-xdata/x)); % function
[x,resnorm,residual,exitflag,output] =
lsqcurvefit(fun,x0,xdata,ydata);
```

```
times = linspace(xdata(1),xdata(end));

figure('Name','4-methylsyringol')
plot(xdata,ydata,'ko',times,fun(x,times),'b-')
legend('Data','Fit')
title('4-methylsyringol: Absorbance vs Time')
xlabel('Time')
ylabel('Absorbance')

% Syringaldehyde
% off
xdata = [25 50 75 100 200 275 375]; %time
ydata = [0.06 0.07 0.075 0.08 0.085 0.095 0.1]; %
absorbance
x0 = [10]; % initial value
Amax = 0.12;

fun = @(x,xdata)Amax*(1-exp(-xdata/x)); % function
[x,resnorm,residual,exitflag,output] =
lsqcurvefit(fun,x0,xdata,ydata);

times = linspace(xdata(1),xdata(end));

figure('Name','Syringaldehyde')
plot(xdata,ydata,'ko',times,fun(x,times),'b-')
legend('Data','Fit')
title('Syringaldehyde: Absorbance vs Time')
xlabel('Time')
ylabel('Absorbance')

% Pyrogallol

xdata = [1 50 75 100 150 200 225]; %time
ydata = [0.001 0.21 0.4 0.41 0.42 0.45 0.48]; % absorbance
x0 = [10]; % initial value
Amax = 0.5;

fun = @(x,xdata)Amax*(1-exp(-xdata/x)); % function
[x,resnorm,residual,exitflag,output] =
lsqcurvefit(fun,x0,xdata,ydata);

times = linspace(xdata(1),xdata(end));
```

```
figure('Name','Pyrogallol')
plot(xdata,ydata,'ko',times,fun(x,times),'b-')
legend('Data','Fit')
title('Pyrogllol: Absorbance vs Time')
xlabel('Time')
ylabel('Absorbance')

% Catechol

xdata = [1 25 50 75 100 150 180]; %time
ydata = [0.001 0.04 0.052 0.08 0.1 0.15 0.18]; % absorbance
x0 = [10]; % initial value
Amax = 0.19;

fun = @(x,xdata)Amax*(1-exp(-xdata/x)); % function
[x,resnorm,residual,exitflag,output] =
lsqcurvefit(fun,x0,xdata,ydata);

times = linspace(xdata(1),xdata(end));

figure('Name','catechol')
plot(xdata,ydata,'ko',times,fun(x,times),'b-')
legend('Data','Fit')
title('catechol: Absorbance vs Time')
xlabel('Time')
ylabel('Absorbance')

% Resorcinol

xdata = [1 25 50 75 100 150 200 250]; %time
ydata = [0.001 0.07 0.1 0.14 0.2 0.3 0.3 0.32]; %
absorbance
x0 = [10]; % initial value
Amax = 0.35;

fun = @(x,xdata)Amax*(1-exp(-xdata/x)); % function
[x,resnorm,residual,exitflag,output] =
lsqcurvefit(fun,x0,xdata,ydata);

times = linspace(xdata(1),xdata(end));

figure('Name','Resorcinol')
plot(xdata,ydata,'ko',times,fun(x,times),'b-')
legend('Data','Fit')
```

```
title('Resorcinol: Absorbance vs Time')
xlabel('Time')
ylabel('Absorbance')

% 3,4-dimethoxybenzaldehyde

xdata = [1 50 100 150 200 300 400]; %time
ydata = [0.006 0.009 0.011 0.014 0.02 0.024 0.029]; %
absorbance
x0 = [10]; % initial value
Amax = 0.03;

fun = @(x,xdata)Amax*(1-exp(-xdata/x)); % function
[x,resnorm,residual,exitflag,output] =
lsqcurvefit(fun,x0,xdata,ydata);

times = linspace(xdata(1),xdata(end));

figure('Name','3,4-dimeth')
plot(xdata,ydata,'ko',times,fun(x,times),'b-')
legend('Data','Fit')
title('3,4-dimethoxybenzaldehyde: Absorbance vs Time')
xlabel('Time')
ylabel('Absorbance')

% Benzaldehyde

xdata = [1 100 200 950]; %time
ydata = [0.0001 0.01 0.013 0.03]; % absorbance
x0 = [10]; % initial value
Amax = 0.32;

fun = @(x,xdata)Amax*(1-exp(-xdata/x)); % function
[x,resnorm,residual,exitflag,output] =
lsqcurvefit(fun,x0,xdata,ydata);

times = linspace(xdata(1),xdata(end));

figure('Name','Benzaldehyde')
plot(xdata,ydata,'ko',times,fun(x,times),'b-')
legend('Data','Fit')
title('Benzaldehyde: Absorbance vs Time')
xlabel('Time')
ylabel('Absorbance')
```

Appendix 2c

Error analysis

```
clc;
clear all
close all

% time data for 6 compounds
xd =
{[0.0100000000000000,45,140,252],[1,100,200,300,400],[1,25,
50,75,100,150,200,275],[1,25,50,75,100,150,180],[1,25,50,75
,100,150,180,200,210],[1,25,50,75,100,150,200,380],[25,50,7
5,100,200,275,375],[1,50,75,100,150,200,225],[1,25,50,75,10
0,150,180],[1,25,50,75,100,150,200,250],[1,50,100,150,200,3
00,400],[1,100,200,950]};
%xdata = [25 50 75 100 200 275 375]; %time
%ydata = [0.06 0.07 0.075 0.08 0.085 0.095 0.1]; %
absorbance
% absorbance data for 6 oompounds
yd =
{[0.0100000000000000,0.0200000000000000,0.0400000000000000,
0.0600000000000000],[0.0500000000000000,0.0600000000000000,
0.100000000000000,0.120000000000000,0.140000000000000],[0.0
0100000000000000,0.0200000000000000,0.0450000000000000,0.07
5000000000000,0.125000000000000,0.110000000000000,0.120000
000000000,0.130000000000000],[0.00100000000000000,0.0090000
0000000000,0.0250000000000000,0.0500000000000000,0.07500000
00000000,0.125000000000000,0.135000000000000],[0.0010000000
0000000,0.0200000000000000,0.100000000000000,0.170000000000
000,0.220000000000000,0.380000000000000,0.470000000000000,0
.460000000000000,0.450000000000000],[0.00300000000000000,0.
00500000000000000,0.0100000000000000,0.0170000000000000,0.0
2000000000000000,0.0350000000000000,0.0360000000000000,0.035
0000000000000],[0.0600000000000000,0.0700000000000000,0.075
0000000000000,0.0800000000000000,0.0850000000000000,0.09500
00000000000,0.100000000000000],[0.00100000000000000,0.21000
0000000000,0.400000000000000,0.410000000000000,0.4200000000
00000,0.450000000000000,0.480000000000000],[0.0010000000000
0000,0.0400000000000000,0.0520000000000000,0.08000000000000
00,0.100000000000000,0.150000000000000,0.180000000000000],[
0.00100000000000000,0.0700000000000000,0.1000000000000000,0.
140000000000000,0.200000000000000,0.300000000000000,0.30000
```

```
0000000000,0.320000000000000],[0.00600000000000000,0.009000
00000000000,0.0110000000000000,0.0140000000000000,0.0200000
000000000,0.0240000000000000,0.0290000000000000],[0.0001000
00000000000,0.0100000000000000,0.0130000000000000,0.0300000
000000000]};
%Amax = 0.1;
Amaxd = [0.5 0.47 0.134 0.14 0.5 0.037 0.1 0.5 0.19 0.35
0.03 0.32];
Name = ['phenol','p-
hydroxybenzaldehyde','guaiacol','vanillin','syringol','4-
methylsyringol','Syringaldehyde','Pyrogallol','Catechol','R
esorcinol','3,4-dimethoxybenzaldehyde','Benzaldehyde'];


for j=1:12
    xdata = xd{j};
    ydata = yd{j};
    Amax = Amaxd(j);
    % time vectors (minutes)
    if j == 1 % phenol
        x0 = [1:10:1000];
    elseif j == 12 % benzaldehyde
        x0 = [1:10:10000];
    else
        x0 = [1:1:100]; % initial value
    end
    fun = @(x,xdata)Amax*(1-exp(-xdata/x)); % function
    for i = 1:length(x0)
        [x(i),resnorm(i),residual,exitflag,output] =
lsqcurvefit(fun,x0(i),xdata,ydata);
    end

    figure(j)
    subplot(2,1,1)
    plot(x0,resnorm,'o')
    xlabel('Initial tau')
    ylabel('Error (resnorm)')
    subplot(2,1,2)
    plot(x,resnorm,'o')
    xlabel('Predicted tau')
    ylabel('Error (resnorm)')
end
```

Appendix 2d

Kinetic models

```
clc;
clear all
close all


Co = 10e-6; % Initial concentration
Name = ["phenol" "guiacol" "vanillin" "syringol" "catechol"
"benzaldehyde"];
MW = [94.11 124.14 152.15 154.16 110.1 106.124];
kOH = [1.4e10 4.53e10 4e8 5.82e10 1.1e10 1.26e10];
data_t = {[1,45,140,252]    [1,25,50,75,100,150,200,275]
[1,25,50,75,100,150,180]
[1,25,50,75,100,150,180,200,210]
[1,25,50,75,100,150,180]    [1,100,200,950]};
data_Abs =
{[0.010000000000000,0.020000000000000,0.040000000000000,
0.060000000000000]
[0.001000000000000,0.020000000000000,0.045000000000000,
0.075000000000000,0.125000000000000,0.110000000000000,0.12
0000000000000,0.130000000000000]
[0.001000000000000,0.009000000000000,0.025000000000000
,0.050000000000000,0.075000000000000,0.125000000000000,0.
135000000000000]
[0.001000000000000,0.020000000000000,0.100000000000000,0
.170000000000000,0.220000000000000,0.380000000000000,0.4700
00000000000,0.460000000000000,0.450000000000000]
[0.001000000000000,0.040000000000000,0.052000000000000,
0.080000000000000,0.100000000000000,0.150000000000000,0.18
0000000000000]
[0.000100000000000000,0.010000000000000,0.013000000000000
,0.030000000000000]};

tau =
[146.215906287634,82.9142611991456,117.583007795512,123.103
810377615,112.685475946744,170];
%Ao = [11,30,8,20,17,100];
for w = 1:6
    Ao(w) = data_Abs{w}(1);
end
```

```
rho = 1400;
lambda = 450e-9;
Cm = Co.*MW.*1.1.*2.39;
L = 1e-2;

H2O2o = 1e-6;
% H2O2o = 1e-9;
jH2O2 = 1e-3;
OHo = 0;

Ao = Ao.*1e-3; % VECTOR, 1e-3 conversion to go from 10 mM
to 10 uM
Amax = [0.07 0.134 0.14 0.5 0.19 0.32];
Amax = Amax.*1e-3; %(Co./H2O2o).*(Co./10e-3);



dt = 1;
time = 0:dt:3600*4;

tau = tau.*60; % VECTOR
tau0 = 1./(kOH*H2O2o);
power = round(abs(log10(tau0)))+1;
step = 10.^-power;


%%
A = zeros(length(time),1);
C = zeros(length(time),1)';
H2O2 = zeros(length(time),1)';
OH = zeros(length(time),1)';
% tau = zeros(length(time),1)';

C_old = Co;
H2O2_old = H2O2o;
OH_old = OHo;

for z = 1:6%length(Name)
    %for z = 1
    tic
    for i = 2:length(time)
        C(1) = Co;
```

```
        A(1) = Ao(z);
        H2O2(1) = H2O2o;
        OH(1) = OHo;
%         tau(z) = tau0(z);


        time_loop = time(i-1) + step(z);
        C_old = C(i-1);
        H2O2_old = H2O2(i-1);
        OH_old = OH(i-1);

        while time(i) > time_loop

          H2O2_new = H2O2_old + step(z)*(-jH2O2*H2O2_old);
          OH_new = OH_old + step(z)*(jH2O2*H2O2_old-
kOH(z)*C_old*OH_old);
          C_new = C_old + step(z)*(-kOH(z)*C_old*OH_old);

          time_loop = time_loop + step(z);
          H2O2_old = H2O2_new;
          OH_old = OH_new;
          C_old = C_new;

        end

        C(i) = C_new;
        H2O2(i) = H2O2_new;
        OH(i) = OH_new;

%         tau(i) = 1/(kOH(z)*OH(i));
%         tau(i) = 146*60;

        A(i) = Ao(z) + (Amax(z)-Ao(z))*(1-exp(-
time(i)/tau(z)));


        rho = 1400;
        lambda = 450e-9;
        Cm = Co*MW(z)*1.1*2.39;
        L = 1e-2;
        k_ref(1) =
(log(10)/(4*pi))*((rho*lambda)/(Cm*L))*Ao(z);
        k_ref(i) =
(log(10)/(4*pi))*((rho*lambda)/(Cm*L))*A(i);
```

```
    end

    data_Abs{z} = data_Abs{z}.*1e-3;%(Co/H2O2o)*(Co*10);
    data_k{z} =
(log(10)./(4.*pi)).*((rho.*lambda)./(Cm.*L)).*data_Abs{z};

    % error
    sum = 0;
    t = time;
    for p = 1:length(data_t{z})
        t_in = data_t{z}(p);
        in = find(t==t_in);
        k_in = k_ref(in);
        resnorm = (data_t{z}(p)-k_in)^2;
        sum = sum+resnorm;
    end

    std = sqrt(sum/(length(data_t{z})-1));
    error(z) = std/sqrt(length(data_t{z}));

    figure(z)
    subplot(1,3,1)
    plot(time/60,C/Co,'b','LineWidth',3)
    axis square
    set(gca,'FontSize',20)
    set(gca,'LineWidth',2)
    xlabel('Time (min)','FontSize',30)
    ylabel('Concentration','FontSize',30)

    subplot(1,3,2)
    plot(time/60,A,'r','LineWidth',3)
    axis square
    set(gca,'FontSize',20)
    set(gca,'LineWidth',2)
    xlabel('Time (min)','FontSize',30)
    ylabel('Absorbance (AU)','FontSize',30)
    hold on
    plot(data_t{z},data_Abs{z},'ko')

    subplot(1,3,3)
    plot(time/60,k_ref,'g','LineWidth',3)
    axis square
```

```
    set(gca,'FontSize',20)
    set(gca,'LineWidth',2)
    xlabel('Time (min)','FontSize',30)
    ylabel('k_r_e_f','FontSize',30)
    hold on
    plot(data_t{z},data_k{z},'ko')
    %annotation('textbox',
[0.5,0.1,0.1,0.1],'String',"Standard error is
"+error(z)+"%")

    toc
end
```